

## Relativistic jet acceleration region in a black hole magnetosphere

Masaaki Takahashi<sup>\*</sup>

*Department of Physics and Astronomy, Aichi University of Education, Kariya, Aichi 448-8542, Japan*

Motoki Kino<sup>†</sup>

*Kogakuin University of Technology & Engineering,  
Academic Support Center, 2665-1 Nakano, Hachioji, Tokyo 192-0015, Japan  
and National Astronomical Observatory of Japan 2-21-1 Osawa, Mitaka, Tokyo, 181-8588, Japan*

Hung-Yi Pu<sup>‡</sup>

*National Taiwan Normal University (NTNU),  
No. 88, Sec. 4, Tingzhou Road, Taipei 116, Taiwan, Republic of China; Institute of Astronomy and  
Astrophysics, Academia Sinica, 11F of Astronomy-Mathematics Building, AS/NTU No. 1, Sec. 4, Roosevelt  
Rd, Taipei 10617, Taiwan, Republic of China; and Physics Division, National Center for Theoretical  
Sciences, Taipei 10617, Taiwan, Republic of China*



(Received 2 April 2021; accepted 1 October 2021; published 5 November 2021)

We discuss stationary and axisymmetric transmagnetosonic outflows in the magnetosphere of a rotating black hole (BH). Ejected plasma from the plasma source located near the BH is accelerated far away to form a relativistic jet. In this study, the plasma acceleration efficiency and conversion of fluid energy from electromagnetic energy are considered by employing the transfast magnetosonic flow solution derived by Takahashi & Tomimatsu (2008). Considering the parameter dependence of magnetohydrodynamical flows, we search for the parameters of the transmagnetosonic outflow solution to the recent M87 jet observations and obtain the angular velocity values of the magnetic field line and angular momentum of the outflow in the magnetized jet flow. Therefore, we estimate the locations of the outer light surface, Alfvén surface, and separation surface of the flow. We also discuss the electromagnetic energy flux from the rotating BH (i.e., the Blandford–Znajek process), which suggests that the energy extraction mechanism is effective for the M87 relativistic jet.

DOI: [10.1103/PhysRevD.104.103004](https://doi.org/10.1103/PhysRevD.104.103004)

### I. INTRODUCTION

The system of a supermassive black hole (BH) with accreting matter is widely believed to be the central engine of the galactic nuclei, and relativistic jets are often observed. Recently, very-long baseline interferometry (VLBI) observations have revealed the configuration and velocity distribution of the M87 jet near the BH [1,2]. The parsec-scale jet of the galaxy M87 is parabolic-like [3,4], and it becomes conical-like near the BH [5]. The radial profile of the jet velocity was observed by Park *et al.* [6] using the KVN and VERA Array (KaVA) (KVN: Korean VLBI Network; VERA: VLBI Exploration of Radio Astronomy). The rapid increase in velocity is observed approximately 100 to 1,000 times the BH's radius. This area is called the acceleration region and is considered to extend from slightly inside the outer light surface to the area several times the fast-magnetosonic surface. Thus,

detailed data for the region closer to the base of the jet were obtained. Exploring the base of the jet would advance our understanding of plasma near the BH.

A magnetic field is generated by accretion plasma around the BH, which is dominant around the axis of rotation. Such a region is called the BH magnetosphere. At the low- and mid-latitudes of this rotating system, a gas torus is formed by accretion gas. The outflow is ejected from a plasma source located in the magnetosphere and accelerated by the Lorentz force toward a distant region. The BH magnetosphere extends along the flow from the BH to the region where the magnetic field and the fluid energies become comparable. We consider stationary and axisymmetric magnetohydrodynamic (MHD) outflows in the BH magnetosphere as relativistic jets. Figure 1 shows transfast magnetosonic outflow and inflow in a BH magnetosphere. The flow region (a funnel) is confined by a corona and/or disk wind, and cold MHD flow is considered. It is shown separately for the electromagnetic field component (Poynting flux: blue arrows) and fluid component (red arrows) of the MHD flow's energy flux.

<sup>\*</sup>mtakahas@aecc.aichi-edu.ac.jp

<sup>†</sup>motoki.kino@nao.ac.jp

<sup>‡</sup>hyu@ntnu.edu.tw

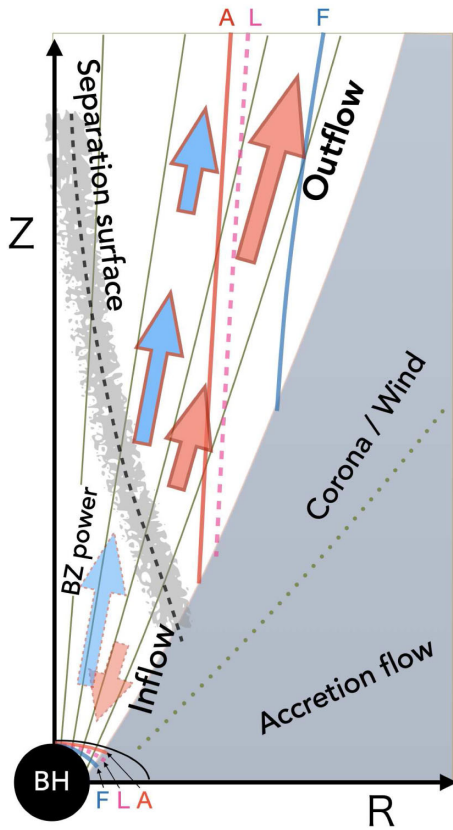


FIG. 1. Schematic of MHD flows driven by rotating BH (BZ power). The thin green curves are the global magnetic field lines in the magnetosphere. The blue and red arrows indicate the direction of the Poynting and fluid component fluxes, respectively. The ejected outflow and inflow from a plasma source, which may be near the separation surface, pass through the Alfvén surface (A), light surface (L), and fast-magnetosonic surface (F) in order, then accelerate toward a distant and the BH, respectively. The thin black curve around the BH is the boundary of the ergosphere.

The jet power derived from the rotational energy of the BH would be explained via the Blandford–Znajek (BZ) process [7,8] (see also, [9,10]). The rotation of the magnetosphere generates a strong centrifugal force on plasma, thereby creating a region that produces an outward plasma flow along a magnetic field line; moreover, there is a region of accretion flow because of strong gravity near the BH. Therefore, there is a plasma supply between the inflow and outflow regions, which is a watershed for inflow and outflow ejected from the plasma source with low velocity and is located between the inner and outer light surfaces (e.g., [11,12]). Thus, the BH magnetosphere can be classified into inner and outer regions; i.e., the inner and outer BH magnetospheres. The region where gravity and centrifugal force act on the plasma along the streamline balance is called the “separation surface,”  $r_{sp}(\theta)$ .

For a stationary and axisymmetric ideal MHD flow solution in the BH magnetosphere, in addition to the

parameters of BH spacetime and the function of the magnetic field shape  $\Psi(r, \theta)$ , the total energy  $E(\Psi)$  and total angular momentum  $L(\Psi)$  of the flow, the angular velocity of the magnetic field lines  $\Omega_F(\Psi)$ , and the particle number flux per magnetic flux tube  $\eta(\Psi)$  should be specified. These parameters are conserved along the magnetic field line (i.e., the flow’s streamline). By analyzing these parameter values for the outflow solution with a solution of magnetic field distribution, various jet morphologies and behaviors would be elucidated. To apply the flow solution to an observed relativistic jet, it is necessary to associate the physical quantity obtained from the observation with the model parameters as the field-aligned conserved quantities.

We examine the nature of the magnetized outflow and then the acceleration of the jet near its base region. Further, we compare the outflow solution with the M87 observed data in the framework of general relativity. We expect this attempt to impose restrictions on unknown plasma sources and inflow onto the BH. Generally, solving the equation of motion for magnetized fluid involves analysis of critical conditions at the Alfvén point as well as fast and slow magnetosonic points under a given magnetic field line. This analysis is complex and tedious (see, e.g., [13–15]). However, Takahashi & Tomimatsu [16] (hereinafter, TT08) analytically devised transmagnetosonic flow solution without a complicated regularity condition analysis at the magnetosonic surfaces. In this study, we adopt the method of TT08 to analyze transfast magnetosonic flow solutions. This method facilitates the analysis of stationary transmagnetosonic flow solutions; i.e., we can easily solve the MHD flows and discuss the distributions of plasma density, the flow velocity, and the ratio of the magnetization of the flow. Hence, we apply the flow solution to the M87 jet.

The asymptotic structures of the magnetic field and relativistic flow have been discussed (e.g., [17–20]). Recently, Huang, Pan & Yu [21] numerically discussed a self-consistent magnetosphere of a BH by solving the transfield equation (the relativistic Grad–Shafranov equation) [22,23] (see also [24]) with the poloidal equation and applied it to the M87 jet to explain the velocity distribution. Kino *et al.* [25] discussed the flow acceleration of the M87 jet by employing an analytical model of Tomimatsu & Takahashi [26] (hereinafter, TT03), which solved the approximated transfield equation outside the outer light surface.

Pu & Takahashi [27] discussed transfast magnetosonic jets in a BH magnetosphere by using TT08, where the injection surface  $r_{inj}(\Psi)$  of flows was set to the location of the separation surface  $r_{sp}(\Psi)$ , and the injected flow starts with a zero velocity,  $u_{inj}^r = 0$ . They performed parameter searches for  $\Omega_F$ ,  $E$ ,  $\Psi$  and the BH spin dependencies. Notably, the angular momentum  $L$  of outflow injected from the separation surface with zero velocity can be described by using other conserved quantities.

In this study, we release such an initial setting for outflows by Pu & Takahashi [27] that restricted the  $L$  parameter, and search the dependence of the values of  $E$ ,  $L$  and  $\Omega_F$  on the jet acceleration motivated by the M87 observations, where the configuration of the magnetic field is considered to be of conical shape for some parameter searches. The parameter search of  $L$  is to allow the flows to have a finite initial velocity ( $u_{\text{inj}}^r > 0$ ) at the separation surface,  $r_{\text{inj}} = r_{\text{sp}}$ , or an initial zero velocity ( $u_{\text{inj}}^r = 0$ ) ejected from the radius of  $r_{\text{inj}} \geq r_{\text{sp}}$ . The specific location of  $r_{\text{inj}}(\theta)$  is still under debate in the BH magnetosphere as the jet base. It could be due to electron-positron pair-creation from the background MeV photons [28–31] or modest acceleration within a charge-starved region at the null surface or the separation surface [32–37]). Recently, the structure of a BH magnetosphere in consideration of the pair-creation near the horizon was studied via general-relativistic particle-in-cell simulations [38,39]. Thus, the initial position and velocity ( $r_{\text{inj}}, u_{\text{inj}}^r$ ), which are associated with the angular momentum  $L$ , are expected to shift from  $r_{\text{inj}} = r_{\text{sp}}$  with  $u_{\text{inj}}^r = 0$  to  $r_{\text{inj}} \neq r_{\text{sp}}$  with  $u_{\text{inj}}^r \neq 0$ .

The rest of this manuscript is organized as follows. In Sec. II, we review the transmagnetosonic flow solutions discussed by TT08. In Sec. III, we summarize the properties of cold transfast magnetosonic flow solutions by analyzing the field-aligned flow parameters. In Sec. IV, we discuss the outflow solution in detail for comparison with the jet observations. The application to the M87 jet is presented in Sec. V, and we discuss it in Sec. VI. Using the physical parameters of the outflow solution obtained by fitting with observed data, we estimate the values of  $E$ ,  $\Omega_F$ , and  $L$ ; i.e., the locations of the outer light surface, Alfvén surface, and separation surface of the outflow. Further, the observed M87 jet power can be explained by the BZ power. The stationary model of magnetically driven jets in a BH magnetosphere would explain the observed properties of the M87 jet and similar low luminosity AGN jets. Finally, we give concluding remarks in Sec. VII.

## II. BASIC EQUATIONS FOR TRANSFAST MAGNETOSONIC FLOW

We assume stationary and axisymmetric ideal MHD flows in a BH magnetosphere in Kerr geometry. The background metric is written by the Boyer–Lindquist coordinates with  $c = G = 1$ ,

$$ds^2 = \left(1 - \frac{2mr}{\Sigma}\right) dt^2 + \frac{4amr \sin^2 \theta}{\Sigma} dt d\phi - \frac{A \sin^2 \theta}{\Sigma} d\phi^2 - \frac{\Sigma}{\Delta} dr^2 - \Sigma d\theta^2, \quad (1)$$

where  $m$  and  $a$  denote the mass and angular momentum per unit mass of the BH, respectively, and  $\Delta \equiv r^2 - 2mr + a^2$ ,

$\Sigma \equiv r^2 + a^2 \cos^2 \theta$ ,  $\mathcal{A} \equiv (r^2 + a^2)^2 - \Delta a^2 \sin^2 \theta$ . The particle number conservation is  $(nu^\mu)_{;\mu} = 0$ , where  $n$  is the number density of the plasma, and  $u^\mu$  is the fluid 4-velocity. The ideal MHD condition is  $u^\nu F_{\mu\nu} = 0$ , where  $F_{\mu\nu}$  is the electromagnetic tensor, and it is written as  $F_{\mu\nu} = A_{\nu,\mu} - A_{\mu,\nu}$  using the vector potential  $A_\mu$ . The relativistic polytropic relation is  $P = K\rho_0^\Gamma$ , where  $\Gamma$  is the adiabatic index,  $K$  is related to the entropy,  $\rho_0 = nm_{\text{part}}$  is the rest mass density, and  $m_{\text{part}}$  is the mass of plasma particles. The equation of motion is  $T^{\mu\nu}{}_{;\nu} = 0$ . The energy–momentum tensor is given by  $T^{\mu\nu} = T_{\text{fluid}}^{\mu\nu} + T_{\text{EM}}^{\mu\nu}$ , where the fluid part is  $T_{\text{fluid}}^{\mu\nu} = n\mu u^\mu u^\nu - P g^{\mu\nu}$ , the electromagnetic part is  $T_{\text{EM}}^{\mu\nu} = (1/4\pi)[F^\mu{}_\lambda F^{\lambda\nu} + (1/4)g^{\mu\nu} F^2]$ ,  $\mu \equiv (\rho + P)/n$  is the relativistic enthalpy,  $\rho$  is the total energy density, and  $F^2 \equiv F^{\mu\nu} F_{\mu\nu}$ .

### A. Relativistic Bernoulli equation for MHD flows

We define the magnetic and electric fields as follows:  $B_\mu \equiv *F_{\mu\nu} k^\nu$  and  $E_\mu \equiv F_{\mu\nu} k^\nu$ , where  $*F_{\mu\nu} \equiv (1/2)\sqrt{-g}\epsilon_{\mu\nu\sigma\lambda} F^{\sigma\lambda}$ , and  $k^\nu = (1, 0, 0, 0)$  is the timelike Killing vector. The poloidal component  $B_p$  of the magnetic field seen by a lab-frame observer is given by

$$B_p^2 \equiv -(B^r B_r + B^\theta B_\theta)/G_t^2 = -[g^{rr}(\partial_r \Psi)^2 + g^{\theta\theta}(\partial_\theta \Psi)^2]/\rho_w^2, \quad (2)$$

where  $G_t \equiv g_{tt} + g_{t\phi}\Omega_F$  and  $\rho_w^2 \equiv g_{t\phi}^2 - g_{tt}g_{\phi\phi} = \Delta \sin^2 \theta$ . The function  $\Psi(r, \theta)$  is the magnetic stream function (the  $\phi$  component of the vector potential,  $A_\phi(r, \theta)$ ). The ideal MHD flow stream along the magnetic field lines,  $\Psi(r, \theta) = \text{constant}$  lines, and have five field-aligned flow parameters; the particle number flux per magnetic flux  $\eta(\Psi) = nu_p/B_p$ , total energy  $E(\Psi) = \mu u_t - \Omega_F B_\phi/(4\pi\eta)$ , total angular momentum  $L(\Psi) = -\mu u_\phi - B_\phi/(4\pi\eta)$ , entropy, and angular velocity of magnetic field lines  $\Omega_F(\Psi) = -F_{tA}/F_{\phi A}$  [40,41]. Thus, we can treat one-dimensional MHD flows along a  $\Psi(r, \theta) = \text{constant}$  line. The physical variables of flows are denoted as a function of  $r$  and  $\Psi$  with field-aligned flow parameters.

We define the poloidal velocity  $u_p$  by  $u_p^2 \equiv -(u^r u_r + u^\theta u_\theta)$ . The relativistic Alfvén Mach number  $M$  is defined by

$$M^2 \equiv \frac{4\pi\mu n u_p^2}{B_p^2} = \frac{\hat{\mu} u_p}{\mathcal{B}_p}, \quad (3)$$

where the term  $\mathcal{B}_p \equiv B_p/(4\pi\mu_c\eta)$  is introduced to non-dimensionalize and  $\mu_c$  is the enthalpy for a cold flow; i.e.,  $\mu_c = m_{\text{part}}$ . The nondimensional toroidal component of the magnetic field  $\mathcal{B}_\phi$  is defined as

$$\mathcal{B}_\phi \equiv \left( \frac{1}{\rho_w} \right) \frac{B_\phi}{4\pi\mu_c\eta} = \frac{G_\phi \hat{E} + G_t \hat{L}}{\rho_w(M^2 - \alpha)}, \quad (4)$$

where  $\hat{E} \equiv E/m_{\text{part}}$ ,  $\hat{L} \equiv L/m_{\text{part}}$ ,  $G_\phi \equiv g_{t\phi} + g_{\phi\phi}\Omega_F$ , and  $\alpha \equiv G_t + G_\phi\Omega_F$ . The toroidal magnetic field  $B_\phi = (\Delta/\Sigma)F_{\theta r}$  can be expressed in terms of the field-aligned flow parameters and Alfvén Mach number. The point of  $M^2 = \alpha$  with  $G_\phi\hat{E} + G_t\hat{L} = 0$  on the flow solution is called the ‘‘Alfvén point’’ (labeled as ‘‘A’’); i.e., the point  $(r_A, M_A^2; \Psi)$  in the  $r$ - $M^2$  plane. At the Alfvén point,  $B_{\phi A}$  has a nonzero finite value. The radius  $r_A$  is called the ‘‘Alfvén radius.’’ Notably, we may identify the radius given by  $G_\phi\hat{E} + G_t\hat{L} = 0$  without  $M^2 = \alpha$ . Such a radius is called an ‘‘anchor radius’’ for the magnetic field line considered (TT08), where  $B_\phi = 0$ . Although the magnetic field line in an axisymmetric magnetic surface (i.e.,  $\Psi = \text{constant}$  surface) has a spiral shape in the toroidal direction, the direction of winding is reversed at the anchor radius if such a radius appears on the magnetic surface. Both the Alfvén and anchor radii can be located between the inner and outer light surfaces (i.e., the  $\alpha(r, \theta) > 0$  region), where the two light surfaces are given by the locations  $\alpha(r, \Psi; \Omega_F, a) = 0$ .

The relativistic Bernoulli equation for MHD flows, which determines the poloidal velocity (or the Alfvén Mach number) along a magnetic field line, can be expressed as follows: [11,16,42]

$$\hat{e}^2 = \hat{\mu}^2\alpha + M^4(\alpha\mathcal{B}_p^2 + \mathcal{B}_\phi^2), \quad (5)$$

where  $\hat{e} \equiv \hat{E} - \Omega_F\hat{L}$ . The relativistic enthalpy  $\hat{\mu}$  is expressed in terms of  $u_p$  and  $B_p$

$$\hat{\mu} \equiv \frac{\mu}{m_{\text{part}}} = 1 + \left( \frac{\mu_{\text{inj}}}{m_{\text{part}}} \right) \left( \frac{B_p}{u_p} \right)^{\Gamma-1} = 1 + \mu_{\text{hot}} \left( \frac{B_p}{u_p} \right)^{\Gamma-1}, \quad (6)$$

where  $\mu_{\text{hot}} \equiv (\mu_{\text{inj}}/m_{\text{part}})(4\pi\mu_c\eta)^{\Gamma-1}$ , and the term  $\mu_{\text{inj}}$  is evaluated at the plasma injection point by

$$\mu_{\text{inj}} \equiv \frac{\Gamma K}{\Gamma - 1} (m_{\text{part}}\eta)^{\Gamma-1} = \frac{\Gamma}{\Gamma - 1} \frac{P_{\text{inj}}}{n_{\text{inj}}m_{\text{part}}} \left( \frac{u_p^{\text{inj}}}{B_p^{\text{inj}}} \right)^{\Gamma-1}. \quad (7)$$

Now, to solve the relativistic Bernoulli equation (5), we introduce the function  $\beta(r; \Psi)$  as follows: [16]

$$\beta \equiv \frac{\mathcal{B}_\phi}{\mathcal{B}_p}, \quad (8)$$

i.e., the pitch angle of a magnetic field line on a magnetic flux surface. Moreover, we can introduce the poloidal electric-to-toroidal magnetic field amplitude ratio  $\xi(r, \theta) \equiv \bar{E}_p/|\bar{B}_T|$ , seen by a zero angular momentum

observer (ZAMO), where  $\bar{E}_p^2 \equiv -(\bar{E}_r\bar{E}^r + \bar{E}_\theta\bar{E}^\theta)$  and  $\bar{B}_T^2 \equiv -\bar{B}_\phi\bar{B}^\phi$ . The electric and magnetic fields measured by ZAMO are  $\bar{E}_\alpha \equiv F_{\alpha\beta}h^\beta$  and  $\bar{B}_\alpha \equiv (1/2)\eta_{\alpha\beta\gamma\delta}h^\beta F^{\gamma\delta}$  with  $h^\beta = (\Sigma\Delta/\mathcal{A})^{-1/2}(1, 0, 0, \omega)$ . The function  $\xi(r, \theta)$  is related to the above function  $\beta(r, \theta)$ , as  $\xi^2 = -g_{\phi\phi}(\Omega_F - \omega)^2/\beta^2$ , where  $\omega \equiv -g_{t\phi}/g_{\phi\phi}$ .

By assuming the functions of the magnetic field line  $\Psi = \Psi(r, \theta)$  and  $\beta = \beta(r, \theta)$  [or  $\xi = \xi(r, \theta)$ ], we can specify the cross-section of the magnetic flux tube of the MHD flow. Hence, using Eqs. (4) and (5) can be expressed in terms of  $M^2$  and  $\beta$  with the conserved quantities. Although the ratio  $\beta$  should be determined by solving the transfield equation with the poloidal equation self-consistently, in this study, we only consider a magnetic flux tube with a certain functional form of  $\beta(r, \theta)$ . Notably, the function  $\beta(r; \Psi)$  must satisfy certain restrictions at several characteristic locations in a BH magnetosphere (TT08).

## B. Cold MHD flow solutions

The Alfvén Mach number and poloidal velocity along the flow are obtained by solving Eq. (5) with Eq. (4), which is a higher-order equation for  $M^2$  (or  $u_p$ ). However, for a cold MHD flow ( $P = 0$ ), we obtain the following quadratic equation for  $M^2$ : [16]

$$AM^4 - 2BM^2 + C = 0, \quad (9)$$

where

$$A = -(k+1) - \frac{1}{\beta^2\rho_w^2}(G_\phi\hat{E} + G_t\hat{L})^2, \quad (10)$$

$$B = \hat{e}^2 - \alpha, \quad (11)$$

$$C = \alpha(\hat{e}^2 - \alpha), \quad (12)$$

with  $k \equiv (g_{\phi\phi}\hat{E}^2 + 2g_{t\phi}\hat{E}\hat{L} + g_{tt}\hat{L}^2)/\rho_w^2$ . The Alfvén Mach number of the flow is obtained using the following:

$$M_{(\pm)}^2 = \frac{B \pm \sqrt{B^2 - AC}}{A}, \quad (13)$$

where  $M_{(+)}^2 (> \alpha)$  denotes the super-Alfvénic flow, and  $M_{(-)}^2 (< \alpha)$  denotes the sub-Alfvénic flow. At the Alfvén point, we see the condition  $\bar{L}\Omega_F = Y_A$  with the definitions  $\bar{L} \equiv \hat{L}/\hat{E}$  and  $Y(r, \theta) \equiv -G_\phi\Omega_F/G_t$ ; therefore, we have  $(B^2 - AC)_A = 0$ , and we confirm that the Alfvén Mach number becomes  $M_A^2 \equiv M_{(+)\text{A}}^2 = M_{(-)\text{A}}^2 = \alpha_A$ . At the light surface, we have  $M_{(-)\text{L}}^2 = 0$  and  $M_{(+)\text{L}}^2 = 2\hat{e}^2/[-(k_L + 1) - \hat{e}^2/\beta_L^2]$ .

For the cold MHD flow, we define two characteristic Alfvén Mach numbers related to the Alfvén and

fast-magnetosonic wave speeds,  $M_{\text{AW}}^2(r, \theta) \equiv \alpha(r, \theta)$ , and  $M_{\text{FW}}^2(r, \theta) \equiv \alpha(r, \theta) + \beta^2(r, \theta)$ , respectively [11,16]. At the light surface, we obtain  $M_{\text{AW}}^2(r_{\text{L}}; \Psi) = 0$  and  $M_{\text{FW}}^2(r_{\text{L}}; \Psi) = \beta^2$ , and at the event horizon  $r_{\text{H}} = m + \sqrt{m^2 - a^2}$ , we have  $M_{\text{AW}}^2(r_{\text{H}}; \Psi) = g_{\phi\phi}(\Omega_{\text{F}} - \omega_{\text{H}})^2 < 0$  and  $M_{\text{FW}}^2(r_{\text{H}}; \Psi) = 0$ , where  $\omega_{\text{H}} = a/(2mr_{\text{H}})$  is the angular velocity of the BH. Hence, the inflow into the BH must be a transfast magnetosonic flow between the Alfvén surface and the event horizon. The location of  $(\alpha)'_{\text{sp}} = 0$ , where the prime is a derivative along a streamline  $()' \equiv \partial_r + (B^\theta/B^r)\partial_\theta$ , makes the separation surface  $r = r_{\text{sp}}(\theta)$ .

For a trans-Alfvénic outflow, we should select  $M^2 = M_-^2 (< M_{\text{AW}}^2)$  in the sub-Alfvénic region of  $\tilde{L}\Omega_{\text{F}} > Y$ , where is the region from the injection point to the outer Alfvén point, whereas  $M^2 = M_+^2 (> M_{\text{AW}}^2)$  is in the super-Alfvénic region of  $\tilde{L}\Omega_{\text{F}} < Y$ , where is the region from the outer Alfvén point to a distant region. The solution of  $M^2 = M_+^2$  in the super-Alfvénic region becomes transfast magnetosonic. Notably, at the fast-magnetosonic point (labeled as ‘‘F’’), the solution of the above quadratic equation does not diverge provided  $\beta(r; \Psi)$  is a smooth function such that we can obtain a transfast magnetosonic solution without the usual critical analysis at the magnetosonic point. However, if there is a location  $A = 0$  along a distant region, the Mach number  $M^2$  begins to diverge there, where the particle number density and the magnetization parameter become zero. To obtain a physical flow solution ejected from the plasma source, we require the condition  $A(r) > 0$  in all areas of the super-Alfvénic flow.

Using the definition of the Alfvén Mach number, the poloidal velocity of the cold flow  $u_p$  is given by

$$u_p^2 = \mathcal{B}_p^2 M^4 = \frac{1}{\beta^2} \frac{(G_\phi \hat{E} + G_t \hat{L})^2}{\rho_w^2 (M^2 - \alpha)^2} M^4, \quad (14)$$

or using the poloidal Eq. (5), we obtain

$$u_p^2 = \frac{\hat{e}^2 - \alpha}{\alpha + \beta^2}. \quad (15)$$

At the light surface, the poloidal velocity is  $u_p = \hat{e}/\beta$ , where we should select  $M^2(r_{\text{L}}) = M_{(+)}^2(r_{\text{L}})$ . Notably,  $M_{(-)}^2(r_{\text{L}}) = 0$  with  $\mathcal{B}_p(r_{\text{L}}) = 0$ ; i.e., the solution  $M^2(r) = M_{(-)}^2(r)$  breaks at the light surface. At the Alfvén and fast-magnetosonic surfaces, we have  $u_p^2(r_{\text{A}}) = u_{\text{AW}}^2(r_{\text{A}})$  and  $u_p^2(r_{\text{F}}) = u_{\text{FW}}^2(r_{\text{F}})$ , respectively, where the 4-velocity of the Alfvén and fast-magnetosonic waves are defined as  $u_{\text{AW}}^2 \equiv \mathcal{B}_p^2 M_{\text{AW}}^4 = (\mathcal{B}_\phi^2/\beta^2)\alpha^2$ , and  $u_{\text{FW}}^2 \equiv \mathcal{B}_p^2 M_{\text{FW}}^4 = (\mathcal{B}_\phi^2/\beta^2)(\alpha + \beta^2)^2$ .

From defining the Alfvén Mach number, the distribution of the particle number density is obtained as follows:

$$n = \frac{4\pi\mu_c \eta^2}{M^2}. \quad (16)$$

The magnetization parameter  $\sigma$ , which is defined as the ratio of the Poynting flux to the total mass-energy flux seen by a ZAMO, is expressed as follows: [43,44]

$$\sigma(r, \theta) = \frac{B_\phi G_\phi}{4\pi\mu\eta u^t \rho_w^2} = -\frac{\hat{e} - \alpha \hat{h}}{\hat{e} - M^2 \hat{h}}, \quad (17)$$

where  $\hat{h} \equiv g^{tt}(\hat{E} - \hat{L}\omega)$ . Thus, the energy conversion between the magnetic and fluid parts of the MHD flow’s energy  $E$  along the streamline is discussed depending on plasma acceleration.

### III. PROPERTIES OF TRANSFAST MAGNETOSONIC FLOWS

Before considering the transfast magnetosonic outflow solution, the classification and constraints of the entire transfast magnetosonic inflow and outflow solutions in the BH magnetosphere is summarized.

For stationary and axisymmetric ideal MHD flows in the cold limit, there are four conserved quantities along the flow. The flow properties are characterized by these parameters with some constraints. In this section, we investigate the characteristics of the transfast magnetosonic flow solution under the constraints.

#### A. Classification of the trans-Alfvénic flows

The magnetic field lines in the magnetosphere around the Kerr BH are dragged toward the rotation of the BH by the dragging effect of spacetime. In particular, the toroidal component of the magnetic field of  $B_\phi \propto (\Omega_{\text{F}} - \omega)$  and the angular momentum of the flows  $L \propto (\Omega_{\text{F}} - \omega_{\text{A}})$  are strongly influenced by the drag of spacetime. The value of the angular momentum of the flow can be specified by the location of the Alfvén point under given  $E$  and  $\Omega_{\text{F}}$ . Trans-Alfvénic MHD flows in a BH magnetosphere can be classified by  $\tilde{L}\Omega_{\text{F}}$ , which gives the constraint on the field-aligned flow parameters at the Alfvén point by the relation  $\tilde{L}\Omega_{\text{F}} = Y_{\text{A}}$ .

The conditions at the Alfvén point can be typed by the spin of a BH  $a$  and the angular velocity of the magnetic field lines  $\Omega_{\text{F}}$ ; i.e., type I ( $\omega_{\text{H}} \leq \Omega_{\text{F}} < \Omega_{\text{F}}^{\text{max}}$ ), type II ( $0 < \Omega_{\text{F}} < \Omega_{\text{H}}$ ), and type III ( $\Omega_{\text{F}}^{\text{min}} < \Omega_{\text{F}} \leq 0$ ), where  $\Omega_{\text{F}}^{\text{min/max}}$  is the minimum/maximum values of  $\Omega_{\text{F}}$  for the existence of the inner and outer light surfaces on the  $\theta = \pi/2$  plane. For types I and III, where  $(\tilde{L}\Omega_{\text{F}})_{\text{min}} < \tilde{L}\Omega_{\text{F}} \leq 1$  with  $E > 0$  and  $L > 0$  for type I and  $L < 0$  for type III, both the inner and outer Alfvén radii appear in the MHD flow solution. For type II, however, there is one Alfvén radius (the inner or outer one) in the solution, and it can be further classified into the following three cases: (a) type IIa:  $0 < \tilde{L}\Omega_{\text{F}} \leq 1$  with  $L > 0$  and  $E > 0$ , (b) type

TABLE I. Classification of the trans-Alfvénic flows and the relation between the flow's total energy  $E$  and angular momentum  $L$ . The condition  $A(r; \Psi) > 0$  in the super-Alfvénic region is considered.

	$\Omega_F^{\min} < \Omega_F \leq 0$	$0 < \Omega_F < \omega_H$	$\omega_H \leq \Omega_F < \Omega_F^{\max}$	
type I	...	...	$(\tilde{L}\Omega_F)_{\min} < \tilde{L}\Omega_F \leq 1$	$E > 0, L > 0$ inflow or outflow
type IIa	...	$0 < \tilde{L}\Omega_F \leq 1$	...	$E > 0, L > 0$ outflow
type IIb	...	$\tilde{L}\Omega_F \leq 0$	...	$E \geq 0, L \leq 0$ inflow
type IIc	...	$1 \leq \tilde{L}\Omega_F$	...	$E \leq 0, L < 0$ inflow
type III	$(\tilde{L}\Omega_F)_{\min} < \tilde{L}\Omega_F \leq 1$	...	...	$E > 0, L < 0$ inflow or outflow

IIb:  $\tilde{L}\Omega_F \leq 0$  with  $L \leq 0$  and  $E \geq 0$  and (c) type IIc:  $1 \leq \tilde{L}\Omega_F$  with  $L < 0$  and  $E \leq 0$  (see also, Table I).

### B. Constraints on transfast magnetosonic outflows

For the relativistic outflow such as the M87 jet, we will handle the flow through the Alfvén surface located outside the separation surface, which is called the outer Alfvén surface. Such a flow has a positive angular momentum ( $L > 0$ ). Hence, we will consider the types I and type IIa cases. The steady magnetosonic flow in the BH magnetosphere has several essential surfaces that characterize its behavior. They include the separation surface, Alfvén surface, light surface, and fast-magnetosonic surface. The outflow ejected from the plasma source passes through these surfaces before reaching the far distant region.

The locations of the Alfvén surface are related to the field-aligned parameters as  $\tilde{L}\Omega_F = Y_A(\Psi)$ , and as a condition that the trans-Alfvénic outflow reaches to a far distant region,  $A(r, \theta) > 0$  should be required along the flow ( $r_A < r < \infty$ ), as mentioned in the previous section. That is, at the outer Alfvén surface  $r = r_A$ , we find the restriction

$$A(r_A; \Psi) = -k_A - 1 > 0. \quad (18)$$

This imposes a limit on the field-aligned flow parameters. Thus, we have the condition

$$M_A^2 = \alpha_A > \frac{G_{tA}^2}{\hat{E}^2}, \quad (19)$$

and we obtain the minimum energy for the trans-Alfvénic outflows,

$$\hat{E}^2 > \frac{G_{tA}^2}{\alpha_A} = \frac{G_{tA}}{1 - \tilde{L}\Omega_F} \equiv \hat{E}_{\min}^2. \quad (20)$$

Although the function  $A(r; \Psi)$  includes the function  $\xi^2$ , the condition for the minimum energy (20) does not depend on the detail expression of  $\xi^2(r, \theta)$ ; i.e., the minimum energy for jets does not limit the shape of the magnetic field as  $\xi_A^2(r, \theta)$ . Notably, depending on the functional form of  $\xi^2$ ,

there may be a situation where  $A = 0$  with  $M^2 \rightarrow \infty$  in the radius to infinity. For a trans-Alfvénic outflow solution, if  $A = 0$  before reaching the distant region, it becomes unphysical, unless MHD shock [43–45] or some type of MHD instability (e.g., [46]) occurs in the flow. As discussed in TT03, the condition  $\xi^2(r, \theta) < 1 - (1/\hat{E}^2) \equiv \xi_{\text{cr}}^2$  is required to reach a far distant region. In the BH magnetosphere, the condition that the radius of  $A = 0$  does not appear in the transfast magnetosonic solution requires restrictions on  $\tilde{L}\Omega_F$  and  $\xi^2$ . At the location of the  $A = 0$  surface, we have the following functions

$$(\tilde{L}\Omega_F)^\pm(r; \Psi) = \frac{Y}{1 + Y + X} \left\{ 1 + X \pm \left[ 1 + (1 - Y)X - (1 + Y + X) \frac{G_t}{\hat{E}^2} \right]^{1/2} \right\}, \quad (21)$$

where  $X \equiv g_{\phi\phi} G_t (1 - \xi^2) / \rho_w^2$ . For  $M^2$  not to diverge on the way to the distant region, the condition,  $\tilde{L}\Omega_F = Y_A < (\tilde{L}\Omega_F)_A^+ < 1$ , must be satisfied at the Alfvén surface.

Here, the ratio of the toroidal to poloidal magnetic fields is introduced as a model of the magnetic field line shape by the function  $\beta^2(r; \Psi)$ . As a simple situation of the poloidal magnetic field, it may be assumed that a magnetic flux tube is distributed along one conical magnetic flux surface  $\Psi(\theta_0) = \text{constant}$ , where  $\theta_0$  is the angle of the magnetic surface to be considered, and it shows a spiral shape on this sheet. Notably, because the functional form of the magnetic surface  $\Psi(r, \theta)$  in the entire magnetosphere is not given, the cross-sectional area of the magnetic flux tube along the magnetic flux surface may differ from that of the monopole (or split-monopole) magnetosphere. In the conventional study of transmagnetosonic flow solution, one transmagnetosonic solution was selected from the solution curve group generated by combining field-aligned parameters and give the critical condition at the magnetosonic point. On the other hand, the handling introduced here has the merit that by giving a regular function  $\beta^2(r; \Psi)$  [or  $\xi^2(r; \Psi)$ ], a transmagnetosonic flow can be solved without fine-tuning the critical values of the field-aligned flow parameters at the magnetosonic point.

### C. Constraints on magnetic field lines

In the following, the function form of  $\xi^2(r; \Psi)$  [instead of  $\beta^2(r, \theta)$ ] is assumed to be a regular function at the magnetosonic surface, and the magnetized plasma flows depending on the field-aligned conserved flow parameters are considered. Although the toroidal component of magnetic field  $B_\phi(r; \Psi)$  is specified by combining the field-aligned parameters, the cross-sectional area change along the flow is also specified accordingly. Moreover, the acceleration efficiency and the magnetization parameter in the flow are determined depending on the function  $\xi^2(r; \Psi)$  and the field-aligned parameters. As the functional form of  $\xi^2(r, \theta)$ , the one considered in TT03 and TT08 is introduced.

From the condition  $A(r, \theta) > 0$  for the transmagnetosonic flow solution, we have

$$\xi^2(r, \theta) < (k+1) \frac{g_{\phi\phi}(\Omega_F - \omega)^2 \rho_w^2}{(G_\phi \hat{E} + G_t \hat{L})^2} = \frac{-(k+1)}{g'' \hat{E}^2 (1 - \tilde{L} \Omega_F / Y)^2}. \quad (22)$$

At the far distant region ( $r/m \gg 1$ ), this condition becomes

$$\xi^2(r, \theta) < 1 - \frac{1}{\hat{E}^2} + \frac{1}{\hat{E}^2} \frac{2m}{r} + O(r^{-2}). \quad (23)$$

(This corresponds to  $\zeta_0 < (1/\hat{E}^2)(2m/r)$ , where  $\zeta_0$  is introduced in Eq. (A3) of TT08.) Referencing TT03 and TT08, we consider the following  $\xi^2$  model for each type of BH magnetosphere. For the outflows of type I/III/IIa, we can apply the following as a functional form of  $\xi^2(r; \Psi)$ ,

$$\xi^2 = 1 - \frac{\Delta}{\Sigma} \frac{1}{\hat{E}^2} + \zeta. \quad (24)$$

The effect of  $\zeta$  is related to the energy conversion efficiency of the outflow, and discussed in [27]. Assuming  $\zeta = 0$  for simplicity, the radial velocity by Eq. (15) becomes

$$(u^r)^2 = \frac{[\hat{E}^2(1 - \tilde{L}\Omega_F)^2 - \alpha][\hat{E}^2 - (\Delta/\Sigma)]}{\hat{E}^2(\Sigma^2/A) - \alpha}. \quad (25)$$

At a distant region ( $R \equiv r \sin \theta \gg 1$ ), the terminal velocity of the transat magnetosonic relativistic jet becomes  $(u^r)_\infty = \gamma_\infty \sim \hat{E}$ . Thus, the total energy is primarily kinetic in the distant region. On the way to the distant region, the initially magnetically dominated MHD flow energy is converted to the kinetic energy of the plasma.

When we discuss the inflows, certain restrictions on  $\xi^2$  should be considered (TT08). First, it must be  $\xi^2 = 1$  on the event horizon. For example, for type I or III inflow case, we can set up the following functional form:

$$\xi^2 = 1 - \frac{\Delta}{\Sigma} f(r, \theta), \quad (26)$$

where the function  $f(r, \theta)$  is a regular function. When the anchor radius appears in the flow, where the toroidal magnetic field becomes 0, it is necessary to satisfy the condition  $\xi^2 = \infty$  (or  $\beta^2 = 0$ ). Therefore, we can consider the following as an example,

$$\xi^2 = \left(1 - \frac{\Delta}{\Sigma} f(r, \theta)\right) \frac{(G_\phi \hat{E} + G_t \hat{L})_H^2}{(G_\phi \hat{E} + G_t \hat{L})^2}. \quad (27)$$

For type II case, the ‘‘corotation radius’’ defined by the radius of  $\omega(r; \Psi) = \Omega_F$  occurs in the BH magnetosphere. At the corotation radius where  $G_\phi(r; \Psi) = 0$ , we obtain the finite poloidal velocity; i.e.,  $(u^r)^2 = \text{finite}$ , but we get  $M^2 = 0$  where  $n = \infty$  and  $\mathcal{B}_p = \infty$  (i.e.,  $\beta^2 = 0$  with  $\mathcal{B}_\phi = \text{finite}$ ) if  $\xi^2(r; \Psi) = \text{finite} \neq 0$  is assumed. This indicates the breakdown of the flow solution there. Therefore, we require  $\xi^2 = 0$  with  $\beta^2 = \text{finite}$  at the corotation radius. Thus, for type II flows, we can introduce the following functional form:

$$\xi^2 = \left(1 - \frac{\Delta}{\Sigma} f(r, \theta)\right) \left(\frac{\omega - \Omega_F}{\omega_H - \Omega_F}\right)^2. \quad (28)$$

For type IIa outflows (discussed in Sec. IV), the above solution (15) can be applied in the area outside the corotation radius, where  $G_\phi > 0$ . Fortunately, because the separation surface is located outside the corotation radius, there should be no problem with the general outflow, starting from the plasma source located near the separation surface. However, to obtain physical inflow solution (i.e., type IIb/IIc) starting around the separation surface, we must set up  $\xi^2 = 0$  at the corotation radius, hence we should use Eq. (28) as a model of  $\xi^2$  rather than Eq. (26). In the following sections, we focus only on outflows ejected from outside the corotation radius as the jet model.

### D. Injection surface and initial velocity

The outgoing and ingoing plasma flows are injected into the outer and inner BH magnetospheres from the plasma source, respectively. The plasma source must be located between the inner and outer light surfaces so that  $\alpha_{\text{inj}} > 0$  is required. At the injection surfaces  $r = r_{\text{inj}}(\theta)$  with  $M_{\text{inj}}^2 \ll 1$ , from Eq. (9), we have the relation of  $\alpha_{\text{inj}} = (\hat{E} - \hat{L}\Omega_F)^2$ . Because the particle number flux per magnetic flux tube  $\eta(\Psi)$  is the conserved quantity along a magnetic field line, for an injected plasma from the injection surface with a low velocity  $u'_{\text{inj}} \ll 1$ , the number density of flow is very high  $n_{\text{inj}} \gg 1$ . If  $\alpha_{\text{inj}} > (\hat{E} - \hat{L}\Omega_F)^2$ , we have  $(u'_{\text{inj}})^2 < 0$ ; i.e., there is no physical solution that

flows out from the injection surface with a finite initial velocity. Specifically, for a highly magnetized flow of  $\tilde{L}\Omega_F \sim \hat{E}$ , the physical flow would start near the light surface,  $r_{\text{inj}} \lesssim r_L$ . Meanwhile, for a small value of the angular momentum,  $|\hat{L}| < (\hat{E} - \sqrt{\alpha_{\text{inj}}})/|\Omega_F|$ , the flow ejected from the injection surface initially has a relativistic speed (i.e.,  $u_{\text{ini}}^r \gtrsim 1$ ).

#### IV. PARAMETER DEPENDENCIES ON MHD OUTFLOW

We consider the parameter dependence of outflow in detail. For numerical plots of the radial velocity  $u^r(r; \Psi)$  about outflows, we set up the functional form of  $\xi^2(r; \Psi)$ . Hence, from Eq. (13), we obtain the distribution  $M^2(r; \Psi)$  along the flow line; using Eq. (4), we have the toroidal component of the magnetic field  $\mathcal{B}_\phi(r; \Psi)$  and  $\mathcal{B}_p(r; \Psi)$ . As such, assuming the function  $\xi^2(r, \theta)$  is equivalent to assuming the poloidal magnetic field  $\mathcal{B}_p$ . We discuss transfast magnetosonic flow solutions along a single flux tube that is theoretically and observationally valid so that we can consider the qualitative understanding of the behavior of jet flow acceleration.

Certain physical parameters would be significantly affected by the general-relativistic effect; hence, we focus our research on this. The locations of the light and Alfvén surfaces, which are the typical scales of the magnetosphere, primarily depend on the angular velocity  $\Omega_F$  of the magnetic field lines and the ratio of the rotational energy to the total energy  $\tilde{L}\Omega_F$  of the plasma flow, respectively. In the following parameter search, the dependency of  $\Omega_F$  and  $\tilde{L}$  is particularly examined. We assume  $\Omega_F(\Psi) = \text{constant}$  for the entire magnetosphere. Although an example of

$\Omega_F(\Psi) = \text{nonconstant}$  is considered by Pu & Takahashi [27], the basic properties are similar, whereas the distributions of the light surfaces differ slightly. Moreover, we assume  $\eta(\Psi) = \text{constant}$  for the entire magnetosphere for simplicity. Notably, in the  $\xi^2$  model, the parameter  $\eta$  is renormalized into the magnetic field  $\mathcal{B}_p$  and  $\mathcal{B}_\phi$  so that it does not directly appear in the expression of the MHD flow equations.

Figure 2 shows the velocity distribution  $u^r(R, Z)$  when Eq. (24) is employed as the distribution of  $\xi^2(R, Z)$  with constant  $\hat{E}$  and  $\Omega_F$  for a rapidly rotating BH (type IIa) case, where  $R = r \sin \theta$  and  $Z \equiv r \cos \theta$ . To understand the angular momentum dependence on the flow, the cases of constant angular momentum  $\hat{L}(\theta) = \text{constant}$  are plotted in Figs. 2(a) and 2(b), and the case where  $\hat{L}$  has angular dependence of  $\hat{L}(\theta) = \hat{L}_0 \sin^2 \theta$  with a constant  $\hat{L}_0$  is plotted in Fig. 2(c). The outflow from the plasma source (e.g., points P, Q, and R in Fig. 2) flows out in the distant region.

If  $\hat{L}(\theta) = \text{constant}$  in the magnetosphere, the higher the latitude, the smaller the initial velocity. However, when the angular momentum is very large, the flow's forbidden region (i.e.,  $u_p^2 < 0$  region) appears in the high latitude region [see, the shaded region in Fig. 2(b)]. Alternatively, the angular momentum at high latitudes should be selected not too large for the transfast magnetosonic solution to fill the magnetosphere in the jet region [see, Fig. 2(a)]. Moreover, we observe that the behavior of acceleration differs depending on whether the angular momentum is constant throughout the magnetosphere or whether it has a  $\sin^2 \theta$  dependence [see, Fig. 2(c)]. To fit the acceleration profile of the M87 jet (see Fig. 6),  $\tilde{L}\Omega_F = \text{constant}$  seems

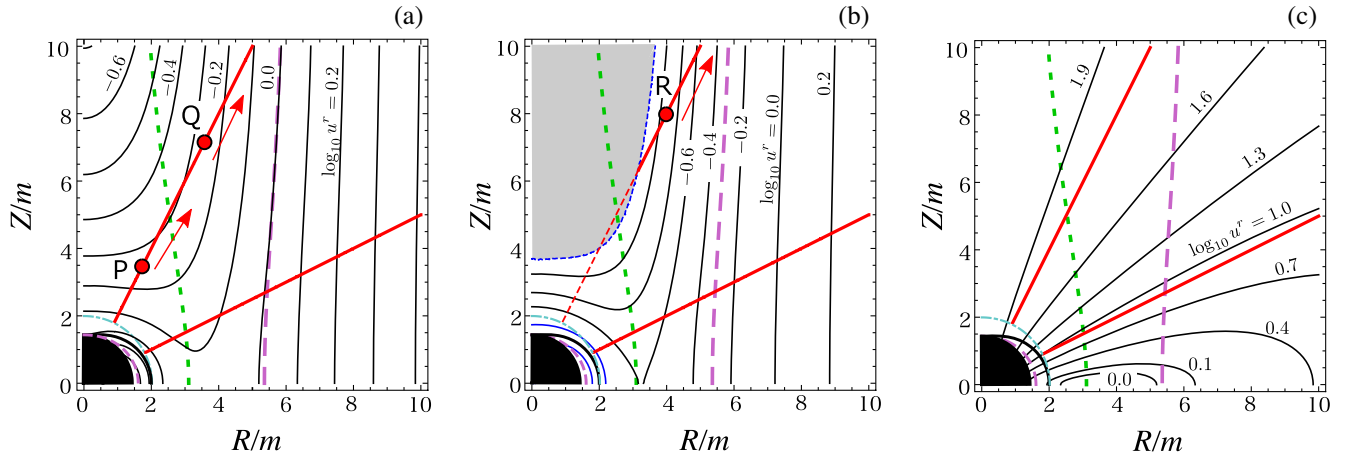


FIG. 2. The distribution of the radial velocity  $u^r(R, Z)$  in the BH magnetosphere of  $a = 0.9m$ ,  $\Omega_F = 0.5\omega_H$ ; (a) the cases of  $\tilde{L}\Omega_F = 0.9$ , (b)  $\tilde{L}\Omega_F = 0.93$ , and (c)  $\tilde{L}(\Psi) = \tilde{L}_0 \sin^2 \theta$ , where  $\tilde{L}_0\Omega_F = 0.9$ . The broken magenta curves show the locations of the inner and outer light surfaces. The dotted green curve shows the location of the separation surface. The shaded area on the upper left of the dotted curve in (b) is the forbidden region, where  $u_p^2 < 0$ . The red lines (outside the corotation surface of the cyan dashed curve) are examples of the streamlines for outflow ( $Z = 2R$ ,  $Z = 0.5R$ ). The red dotted line in (b) is unacceptable as an outflow. The black region shows the BH. Points P, Q, and R are examples of the injection points.

to be better in the entire region of the magnetosphere.

Afterward, we will consider the case of  $\hat{L}(\Psi) = \text{constant}$ .

Figure 2 also shows the velocity distribution within the separation surface, where the parameter set used here corresponds to the type IIa case; therefore, it fails as a physical solution on the corotation surface. Notably, from the area between the corotation and separation surfaces (e.g., point P), an outgoing flow ejected with a sufficiently large initial velocity is possible.

Figures 3–5 show the dependences of the field-aligned parameters on the transfast magnetosonic outflow solutions (red curves) along a  $\theta = \text{constant}$  magnetic field line for the type IIa case. The label “Co” or orange dashed line indicates the location of the corotation surface. The label “SP” or green dotted line indicates the location of the separation surface and the label “LS” or magenta broken lines indicate the location of the light surfaces. The mark  $\square$  labeled “A” and the mark  $\circ$  labeled “F” indicate the Alfvén and fast-magnetosonic points, respectively.

### A. Energy $E$ dependence

In Fig. 3, we show the  $\hat{E}$  dependence on the transfast magnetosonic outflow solutions, where the values of  $a$ ,  $\tilde{L}\Omega_F$ , and  $\Omega_F$  are fixed; therefore, the locations of the separation surface, light surfaces, and Alfvén surfaces are the same. The Alfvén Mach number  $M^2(Z)$  rapidly increases from around the Alfvén point and passes through the fast-magnetosonic point to a distant region. For large  $\hat{E}$  values, where the  $\hat{L}$  value is also large, the location of the fast-magnetosonic point appears on the outside, and the plot of the radial velocity  $u^r(Z)$  shifts upward over the entire area. In Fig. 3(b), the injected plasma around the separation surface has a nonzero initial velocity. For example, the outflow solution passing through point S has an almost constant flow velocity between the corotation and Alfvén surfaces and then accelerates across the fast-magnetosonic surface. For an outflow solution passing through point T, the outflow decelerates once toward the separation surface, but after passing the separation surface, it accelerates and passes through the Alfvén and fast-magnetosonic surfaces in order. For a low energy flow, the plasma flows out at a very low speed from the vicinity of the Alfvén surface (point U), which is far outside the separation surface. Such outflow is significantly accelerated beyond the Alfvén surface from the injection surface.

The rescaled number density  $\tilde{n} \equiv n/(4\pi\mu_c\eta^2) = 1/M^2$  decreases in the distance, unlike the increase in the Alfvén Mach number [see, Fig. 3(a)]. Figure 3(c) shows the distribution of the magnetization parameter  $\sigma(Z)$ . For a large energy outflow, the magnetic field energy is dominant at the beginning of the flow; however, as the outgoing fluid accelerates, the fluid part of the energy increases and becomes dominant at a far distance ( $\sigma \ll 1$ ). For a low energy outflow, which corresponds to a large angular

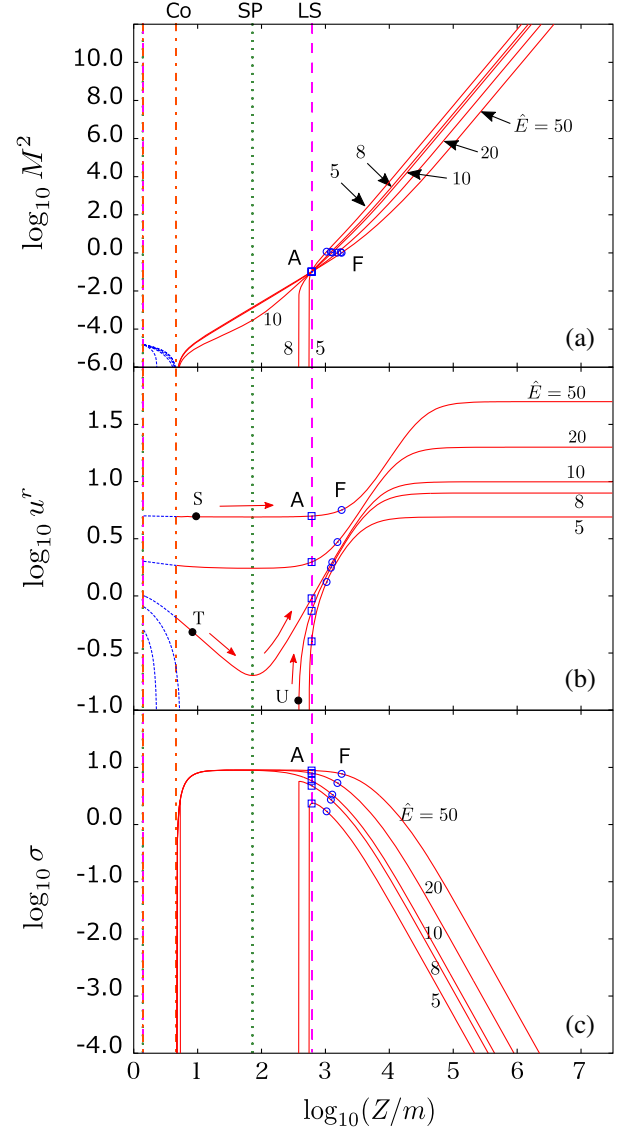


FIG. 3. The dependences of total energy  $\hat{E}$  on relativistic outflows (Type IIa:  $\hat{E} = \{5.0, 8.0, 10.0, 20.0, 50.0\}$  with  $a = 0.9m$ ,  $\Omega_F = 0.05\omega_H = 0.0157/m$ ,  $\tilde{L}\Omega_F = 0.9$ ,  $\theta = 1/\hat{E}$ ) (a) the Alfvén Mach number  $M^2(Z)$ , (b) the radial velocity  $u^r(Z)$  and (c) the magnetization parameter  $\sigma(Z)$ . The blue curves inside the corotation surface (Co) are unphysical solutions as outflows.

momentum outflow, the fluid part of the energy is dominant at the beginning of the flow when the injection point is located just inside the outer light surface.

For a slowly rotating BH case of type I, both the outer light surface and the outer Alfvén surface shift outward; however, the asymptotic feature of outflows is the same.

### B. Angular momentum $\tilde{L}\Omega_F$ ( $L$ ) dependence

Figure 4 shows the  $\tilde{L}\Omega_F$ -dependence on the transfast magnetosonic outflow solutions, where  $\hat{E}$  and  $\Omega_F$  are fixed;

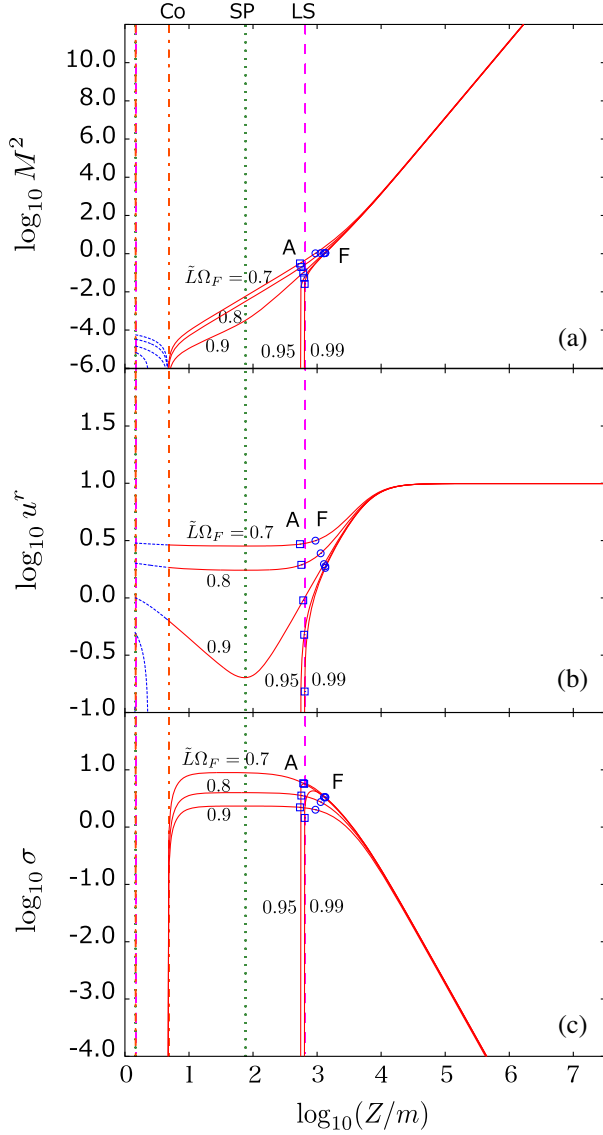


FIG. 4. The dependences of total angular momentum  $\hat{L}$  on relativistic outflows (Type IIa:  $\tilde{L}\Omega_F = \{0.70, 0.80, 0.90, 0.95, 0.99\}$ ,  $a = 0.9m$ ,  $\Omega_F = 0.05\omega_H = 0.0157/m$ ,  $\hat{E} = 10.0$ ,  $\theta = 1/\hat{E}$ ) (a) the Alfvén Mach number  $M^2(Z)$ , (b) the radial velocity  $u^r(Z)$  and (c) the magnetization parameter  $\sigma(Z)$ .

i.e., the dependence of angular momentum  $\hat{L}$  is investigated. The angular momentum  $\hat{L}$  determines the behavior of the initial stage of acceleration of the ejected outflow in the sub-Alfvénic region and near the light surface. For outflows with small angular momentum, the velocity distribution in the sub-Alfvénic region has a large value, i.e., a solution with nonzero velocity is obtained around the separation region. Meanwhile, for outflows with large angular momentum,  $\tilde{L}\Omega_F \sim 1$ , no physical solution region appears around the separation surface in the sub-Alfvénic region. Such a flow with large angular momentum starts at a slower speed from slightly inside the outer light surface,

where the toroidal motion of the flow is dominated; i.e.,  $v_{\text{ini}}^\phi \approx c$  and  $\gamma_{\text{ini}} \gg 1$  (see also, [13]). Thus, the value of  $\hat{L}$  is related to the toroidal motion in the sub-Alfvénic region. The closer the injection surface to the light surface, the more dominant toroidal motion of plasma ( $\sigma_{\text{ini}} \ll 1$ ) is obtained in the initial stage of the MHD flow, whereas the poloidal motion is relatively small. Subsequently, it is converted to poloidal motion, and eventually becomes magnetically dominated MHD outflow ( $\sigma \gg 1$ ) in the next stage of the acceleration region. Through the equipartition region (TT03), the kinetic energy by the poloidal motion becomes dominant over the magnetic energy; i.e.,  $\sigma_\infty \ll 1$ . The terminal velocity  $(u^r)_\infty$  does not depend on angular momentum  $\hat{L}$ . When the angular momentum becomes large, the flow starting near the separation surface is prohibited.

### C. Angular velocity $\Omega_F$ dependence

Figure 5 shows the  $\Omega_F$ -dependence on the transfast magnetosonic outflow solutions, where  $\hat{E}$  and  $\tilde{L}\Omega_F$  are fixed; therefore, a large (or small)  $\Omega_F$  value corresponds to a small (or large)  $\hat{L}$  value. Each solution curve in Fig. 5 is similar, although the location of the light surface depends on both  $\Omega_F$  and  $a$ . When the value of  $\Omega_F$  decreases, the outer light surface shifts to the outside. Meanwhile, when the value of spin  $a$  increases, the effect of the spacetime dragging on the magnetic field lines becomes large and it shifts to the inside.

## V. PLASMA ACCELERATION ON M87 JET

Now, we explain the observed data of the M87 jet by parameter searching using the stationary transfast magnetosonic outflow model. The mass of the central BH in M87 is estimated to be  $m_{\text{M87}} = (6.5 \pm 0.7) \times 10^9 m_\odot$  (e.g., [47,48]). The inclination angle (viewing angle) of the M87 jet is estimated to be  $\theta_{\text{inc}} \approx 17^\circ$  [49]. The jet power in M87 is in a range of  $10^{35} - 10^{37} \text{ J s}^{-1}$ , and there are several theoretical calculations of jet power driven by electromagnetic mechanisms represented by the BZ process [7] and/or Blandford–Payne process [50] (see also, e.g., [51]). The parsec-scale jet of the galaxy M87 is roughly parabolic ( $Z \propto R^{1.7}$ ) in structure [3,4], where  $Z$  is the deprojected distance along the jet, and  $R$  is the jet width, and the M87 jet becomes conical-like ( $Z \propto R^{1.3}$ ) near the BH [5]. The radial profile of the M87 jet velocity is observed by [1,49,52–55], and recently detail data for the region closer to the base of the jet has been obtained by Park *et al.* [6] using the KaVA.

### A. Acceleration region of M87 jet

In this study, we examined the general-relativistic effects in the outer BH magnetosphere. In this section, the M87 jet data fitting is performed using the general-relativistic

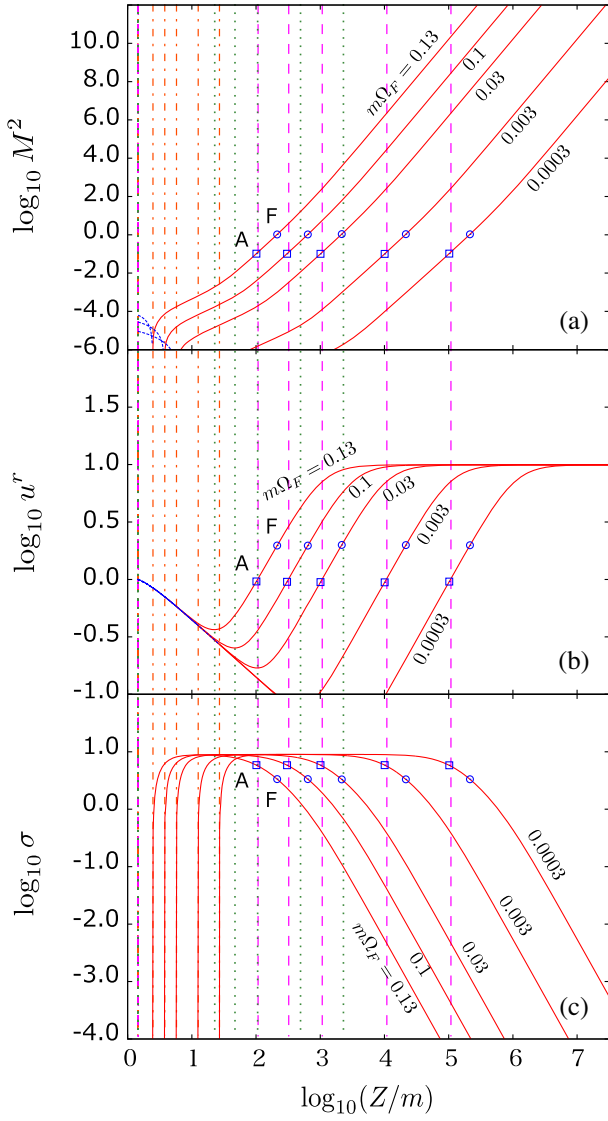


FIG. 5. The dependences of magnetosphere's angular velocity  $\Omega_F$  on relativistic outflows (Type IIa:  $m\Omega_F = \{0.0003, 0.003, 0.03, 0.10, 0.30\}$ ,  $a = 0.9m$ ,  $\hat{E} = 10.0$ ,  $\tilde{L}\Omega_F = 0.9$ ,  $\theta = 1/\hat{E}$ ) (a) the Alfvén Mach number  $M^2(Z)$ , (b) the radial velocity  $u^r(Z)$  and (c) the magnetization parameter  $\sigma(Z)$ .

version of the  $\xi^2$  model by TT08 that incorporates the effect of a rotating BH, where the plausible magnetic field suggested by VLBI observations and general-relativistic MHD (GRMHD) numerical simulations for the relativistic jet are adopted (e.g., [56–58]). To discuss the acceleration properties of the jet, we can consider the angular momentum dependence on the outflow in the acceleration region and the initial velocity around the plasma source region.

In the following, we apply the transfast magnetosonic jet solution to the Park's M87 data [6]. As the flow's streamlines in the BH magnetosphere, we apply the approximated magnetic field configuration in the asymptotic region obtained from Eq. (57) of TT03; i.e.,

$$\theta_0 Z/m = (R/m)^{\Psi_0/\Psi} \quad (29)$$

for  $\theta \ll 1$ , where  $\Psi \rightarrow 0$  for  $\theta \rightarrow 0$ , although this solution should not extend inside the outer light surface because it is out of the range of the approximation of TT03. However, it may be suitable for around the outer light surface, where current observation data are primarily obtained. We expect it to be applicable for qualitative understanding of the relativistic jets from the sub-Alfvénic region of the outer BH magnetosphere. In Fig. 6, we interpolate the approximated magnetic field shape (29) into the sub-Alfvénic region that includes the plasma source, where the boundary layer  $\Psi_0 = \Psi(\theta_0)$  between the jet region and middle/lower latitude accreting matter region is given by the  $\theta_0 \sim 1/\hat{E}$  conical magnetic field line. Notably, around or inside the outer light surface, Hada *et al.* [5] and TT03 model suggests a conical-like magnetic field shape. (The nature of the conical outflow has been discussed in Sec. IV.)

Figures 6(b) and 6(e) show the radial velocity  $u^r(Z)$  of the outgoing jet from the BH magnetosphere. The KaVA's data is rescaled in the unit of  $m_{M87}$ , where  $1\text{mas} \approx 260m_{M87}$  [6]. The correspondence between the apparent angle and actual scale significantly depends on the inclination angle (viewing angle) and opening angle of the jet. The ejected outflow from the plasma source is accelerated around the light surface; after passing the fast-magnetosonic surface, the flow velocity reaches a nearly constant value that is large enough; i.e., the initially magnetically dominated outflow becomes the fluid's kinetic energy dominated flow. Although we assumed that  $a = 0.9m$ , the spin dependence on the outflow solutions is weak at least outside the outer light surface. The efficiency of acceleration differs for each magnetic field line. The magnetic field lines close to the funnel wall ( $\Psi \sim \Psi_0$ ) cause large acceleration; moreover, the acceleration efficiency is minute for the magnetic field lines near the axis ( $\Psi \ll \Psi_0$ ). The plasma source is located near the separation surface of each curve for the magnetic flux surface.

Now, we understand that the values of  $\hat{E}$  and  $\tilde{L}\Omega_F$  are estimated by fitting the terminal velocity  $u_{\infty}^r$  and the initial velocity  $u_{\text{ini}}^r$  at the injection region (or the acceleration region near the plasma source), and the location of the light surface  $r_L$  is specified by parameters  $\Omega_F$  and  $a$ . The transfast magnetosonic MHD outflow becomes a fluid-dominated outflow at the distant region. By observing the terminal velocity  $u_{\infty}^r$  (or  $\gamma_{\infty}$ ) of the M87 jet, we can specify the value of  $\hat{E} \approx 10$ . Angular momentum  $\hat{L}$  (or  $\tilde{L}\Omega_F$ ) is largely related to  $u_{\text{ini}}^r$  and the velocity distribution in the acceleration region around the outer light surface. By comparing the theoretical solution with the M87 observed data, we estimate  $\tilde{L}\Omega_F \approx 0.9$  from the acceleration profile of the jet. If the angular momentum parameter of the flow reduces by some extent, the ejected flow around the separation surface will have a faster initial velocity.

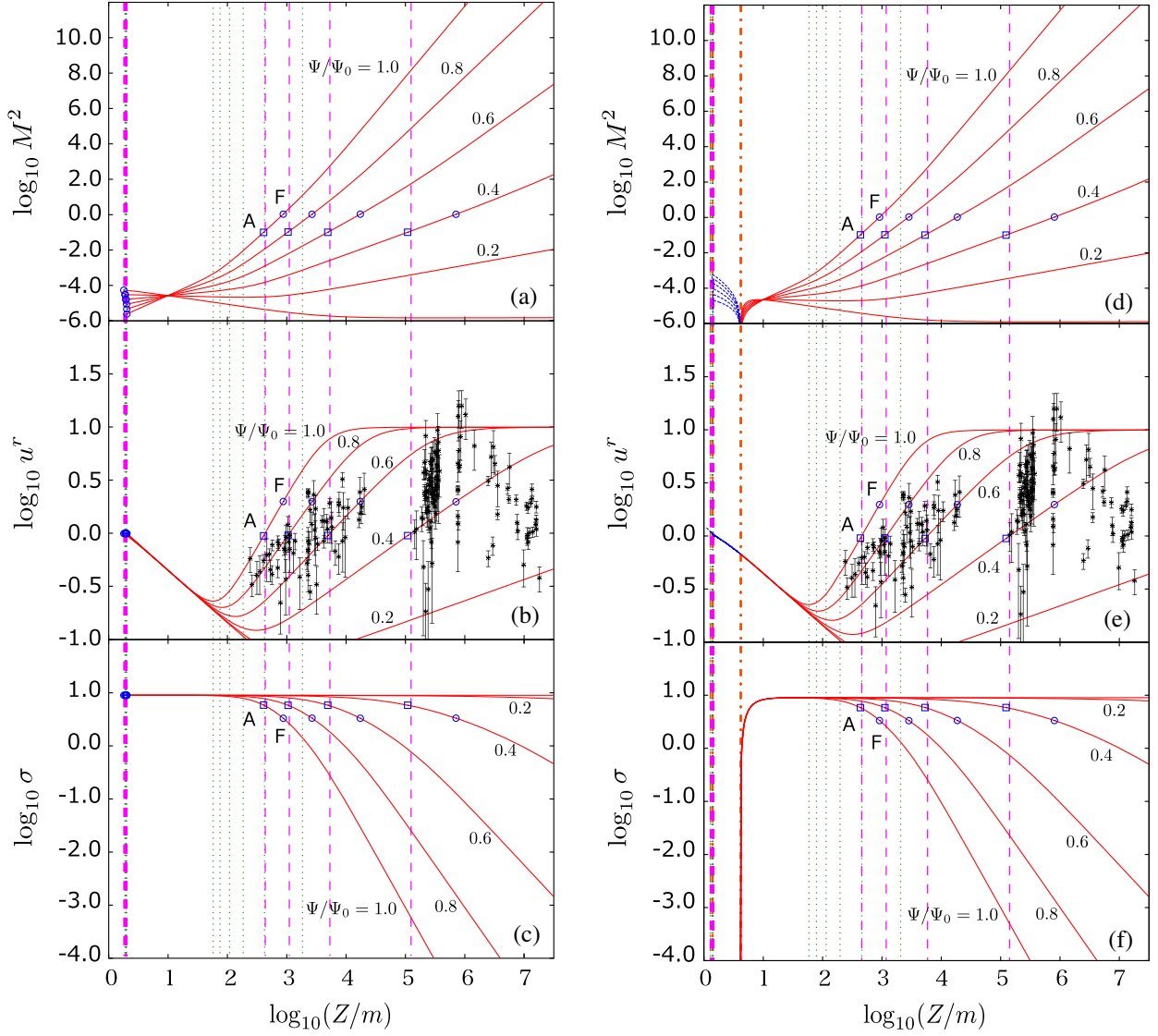


FIG. 6. The  $\Psi$ -dependence on the jet solution is shown ( $\Psi/\Psi_0 = \{1.0, 0.8, 0.6, 0.4, 0.2, 10^{-5}\}$ ,  $\theta_0 = 1/\hat{E}$ ). (a)–(c) type I: a slowly rotating BH of  $a = 0$  with  $\hat{E} = 10.0$ ,  $\Omega_F = \omega_H + 0.12(\Omega_F^{\max} - \omega_H) = 0.0231/m$ ,  $\tilde{L}\Omega_F = 0.9$ , and (d)–(f) type IIa: a rapidly rotating BH of  $a = 0.9m$  with  $\hat{E} = 10$ ,  $\Omega_F = 0.07\omega_H = 0.0219/m$ ,  $\tilde{L}\Omega_F = 0.9$  are presented. The measured data points with error bars are adopted from [6]. In panels (d)(e), the dotted blue curves inside the corotation surface show unphysical branches as the jet solution.

The initial flow acceleration obtained in certain GRMHD simulations (e.g., [2,56,57]) that show  $u_{\text{ini}}^r \gtrsim 1$  and do not explain the M87 observations well would be explained in a parameter range with a small angular momentum.

The location of the outer light surface depends on both the angular velocity of the magnetic field lines and the BH spin. In Figs. 6(b) and 6(e), from the location of the acceleration region for the M87 jet, we estimate that  $\Omega_F \approx 0.023/m$  for  $a = 0$  case, and  $\Omega_F \approx 0.022/m$  for  $a = 0.9m$  case. Thus, the outer light surface,  $R_L \sim c/\Omega_F$ , will be located far enough from the central BH; i.e., the effect of BH spin decreases at the outer light surface. It can be said that the behavior of the jet does not depend on the details of type I or type IIa.

## B. Energy conversion in M87 jet

Figures 6(c) and 6(f) show the distribution of the magnetization parameter  $\sigma(Z)$  in the jet. The efficiency of energy conversion from the magnetic energy to the fluid's kinetic energy differs for each magnetic field line. Although the jet has a large value of  $\sigma$  at the beginning, the value of  $\sigma$  decreases along the magnetic field lines of  $\Psi \sim \Psi_0$ ; then, at a distant region, the jet becomes a kinetic energy-dominated outflow. However, along the magnetic field lines near the axis of rotation,  $\Psi \ll \Psi_0$ , where the centrifugal force on plasma does not work effectively, the acceleration efficiency is relatively small, and the value of  $\sigma$  does not decrease significantly. Thus, the magnetic field lines close to the funnel wall cause efficient energy

conversion, whereas the efficiency is minute for the magnetic field lines near the axis.

The strength of the magnetic field at the footpoint of the jet is estimated from the Event Horizon Telescope (EHT) observation [59,60]. The value of the magnetization parameter  $\sigma$  within the outer light surface is estimated by Kino *et al.* [25]; i.e.,  $1 \times 10^{-5} \leq \sigma \leq 6 \times 10^3$  within the radio core with VLBA at 43 GHz and  $5 \leq \sigma \leq 1 \times 10^6$  within the putative synchrotron self-absorption (SSA) thick region in the EHT emission region at 230 GHz. Thus, we identify that the high values of the  $\sigma$  profile within the outer light surface agree the  $\xi^2$  model for the GRMHD jet.

Moreover, low- $\sigma$  ( $\sigma \sim 10^{-4}$ ) has been observed in the major atmospheric gamma imaging Cherenkov telescope (MAGIC) TeV-gamma observation [61], although the exact location of the gamma-ray emitting region is uncertain. For example, in Fig. 6(c), such a low- $\sigma$  flow can be achieved at a distance of  $Z/m > 10^6$ . Alternatively, the MAGIC observation region may be near the outer light surface, which is because the outflow solution emitted from the region slightly inside the outer light surface is realized with very low- $\sigma_{\text{ini}}$  for  $\tilde{L}\Omega_F \sim 1$  [see, Figs. 3(c) and 4(c)]. Such an outflow initially rotates in the toroidal direction at very high speed ( $\gamma_{\text{ini}} \gg 1$ ), resulting in low- $\sigma$ , and then it accelerates outward. Interestingly, the plasma moving at high speed in the toroidal direction just inside the outer light surface generates an extremely large acceleration, which would be a region where very-high-energy gamma rays are generated. If the vicinity of the outer light surface is the source of high-energy  $\gamma$ -ray for some magnetic field lines in the jet, the  $\gamma$ -ray source may also be distributed along the jet (i.e., hollow cylindrical-shape) because the outer light surface is distributed in the region extending along the jet.

## VI. DISCUSSION

### A. Dependence on magnetic field line shapes

To discuss the parameter dependence of the ideal MHD field-aligned quantities, we assume the magnetic surface has a conical shape. Further, it is easy to extend to other plausible magnetic field shapes; e.g., we can use the model

$$\theta_0 Z/m = (R/m)^{p(\Psi_0/\Psi)}, \quad (30)$$

where  $p$  is a parameter for a magnetic field configuration, and  $\Psi = \Psi_0$  is the streamline for the jet's boundary wall. According to Hada's observation [5], the M87 jet shape near the jet source region bends around the fast-magnetosonic surface, suggesting a conical-like shape on the side near the central BH. This shape would suggest the magnetic field configuration in the BH magnetosphere. When applied to the above model (30), it is about  $p \approx 1.3$  for the boundary wall of the funnel on the inside of the bend and about  $p \approx 1.7$  on the outside.

Figure 7 shows the dependence of the funnel wall configuration of  $p = 1.0, 1.3,$  and  $1.7$ . Hence, one can understand the dependence of the magnetic field shape on the acceleration efficiency of jets. In Fig. 7(a), we plot the radial velocity  $u^r$  for magnetic field lines within the conical boundary wall of  $\theta = \theta_0$ . Figures 7(b) and 7(c) show the cases of parabolic boundary wall of  $p = 1.3$  and  $1.7$ , respectively. When the jet's boundary wall is conical ( $p = 1.0$ ), it is estimated that  $\Omega_F \approx 0.02/m$ , whereas when it is a parabolic shape, the value of  $\Omega_F$  is overestimated

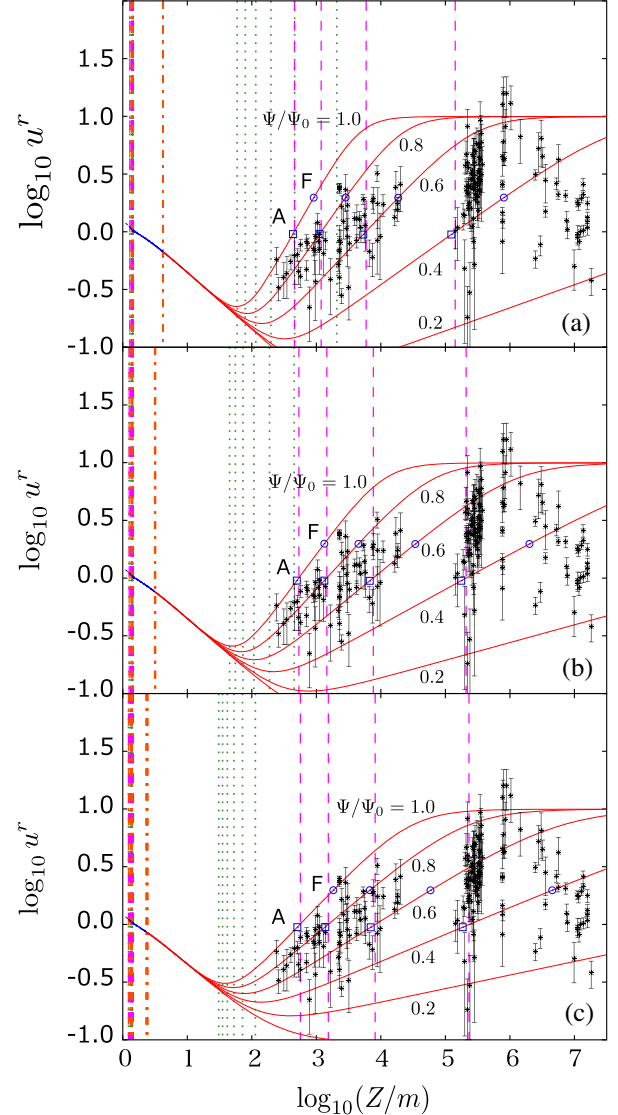


FIG. 7. The radial 4-velocity  $u^r$  of the flow with different magnetic field shapes, (a)  $p = 1.0$ , (b)  $p = 1.3$ , and (c)  $p = 1.7$ , overlapped with the observation jet velocity of M87. The transfast magnetosonic solutions along the magnetic flux surfaces of  $(\Psi/\Psi_0) = \{1.0, 0.8, 0.6, 0.4, 0.2, 10^{-5}\}$  are plotted, where  $a = 0.9m$ ,  $\hat{E} = 10.0$ ,  $\tilde{L}\Omega_F = 0.9$ ,  $\theta_0 = 1/\hat{E}$  and (a)  $\Omega_F = 0.07\omega_H = 0.0219/m$ , (b)  $\Omega_F = 0.15\omega_H = 0.0470/m$ , (c)  $\Omega_F = 0.30\omega_H = 0.0940/m$  are assumed.

compared with the case of conical; i.e.,  $\Omega_F \approx 0.05/m$  for  $p = 1.3$ , and  $\Omega_F \approx 0.09/m$  for  $p = 1.7$ . By fitting with KaVA data within several times  $r_F$ , a value of about  $\Omega_F = (0.02 - 0.05)/m$  is obtained such that it should be slightly parabolic for a slowly rotating BH magnetosphere according to Thoelecke *et al.* [62]. Thus, the model of the magnetic line shape of  $\Psi(r, \theta)$  and  $\xi^2(r; \Psi)$  used in this study incorporates a plausible situation based on the observation results to some extent.

Although Hada *et al.* [5] observed bending of the jet shape, the physical reason for this bending was discussed in TT03. TT03 considered the flow of  $E = \gamma_\infty \gg 1$ , derived the approximated transfield equation for the outer region of the outer light surface, and solved the self-consistent magnetic field configuration. The outflow ejected from the plasma source was initially magnetically dominated. In the process of passing through the Alfvén and fast-magneto-sonic surfaces and accelerating, the energy conversion from magnetic field energy to fluid kinetic energy occurs slowly but effectively. The bending of the magnetic field lines occurs in the area where the energy of both become equipartition. In other words, in the inner region where the magnetic field is dominant, it is conical-like or slightly parabolic, and when the plasma is accelerated and the plasma inertia becomes effective, the toroidal component  $B_\phi$  of the magnetic field is enhanced. Therefore, the magnetic field lines are curved toward the rotation axis. Although the shape of the magnetic field lines in the vicinity of the BH is still unexplored, the observation results of the jet shape (i.e., magnetic field lines) of Hada *et al.* [5] in the region close to the footpoint of the jet seem to roughly correspond to the magnetic field configuration suggested by TT03.

Notably, comparing the parabolic shape with the conical shape, for the same value of  $\Omega_F$ , the location of the outer light surface along the jet,  $Z_L(\Psi_0)$ , shifts in the +Z-direction; however, the width of the outer light cylinder,  $R_L$ , is the same. Even if the  $Z_L(\Psi_0)$  is observably estimated along the streamline of the jet, there is a dependence on both  $\Omega_F$ ,  $p$ , and  $\theta_0$ . If the velocity distribution in the width direction of the jet is measured, the width  $R_L$  (i.e.,  $\Omega_F$ ) can be directly estimated.

### B. M87 jet power and BZ power

The BZ power is obtained from estimating the magnetic field strength near the rotating BH and the angular velocity values (i.e.,  $0 < \Omega_F < \omega_H$ ). It is difficult to estimate the value of the BH spin from the observation data by Park *et al.* [6]. However, the  $\Omega_F^{\text{outflow}}$  value can be estimated from the observation and by assuming the  $\Omega_F$  values match in the outflow and inflow across the plasma source region without significant energy loss. Hence, it can be considered whether BZ power can be applied as the jet power. For example, we can assume the junction condition at the plasma source as  $\Omega_F^{\text{inflow}} \approx \Omega_F^{\text{outflow}}$ , and  $\mathcal{E}_H^r \approx (\eta E)_{\text{outflow}}$ , where  $\mathcal{E}^r \equiv T_{EM}^{\alpha k}$

is the radial component of the conserved electromagnetic energy flux (i.e., BZ power) and  $\eta E$  is the energy flux of MHD flow. For the outflow where  $\eta_{\text{outflow}} > 0$  and  $E_{\text{outflow}} > 0$ ,  $(\eta E)_{\text{outflow}}$  indicates the jet power per magnetic flux. Note that the jet power  $(\eta E)_{\text{outflow}}$  comprises the magnetic and fluid parts of the energy flux, whereas  $\mathcal{E}_H^r$  is purely magnetic energy flux from the BH.

We can also consider the case of  $\mathcal{E}_H^r > (\eta E)_{\text{inflow}} \approx (\eta E)_{\text{outflow}}$  across the plasma source, where  $(\eta E)_{\text{inflow}}$  can be obtained as a solution of type IIc negative energy MHD inflow; i.e.,  $E_{\text{inflow}} < 0$ ,  $L_{\text{inflow}} < 0$ ,  $\eta_{\text{inflow}} < 0$  inflow [11,63] (see also, [30] for gamma-ray bursts jets). Notably,  $\mathcal{E}_H^r \approx (\eta E)_{\text{inflow}} > 0$  in the magnetically dominated limit (i.e., force-free case). For the solution of type IIc inflow, the magnetic field geometry of Eq. (28) should be adopted to avoid the break at the corotation surface during accretion onto the event horizon. Moreover, the boundary conditions at the plasma source that agree with the outflow solution must be estimated within the physical parameter ranges such that  $A(r, \theta) > 0$  between the plasma source and the event horizon.

When the magnetic field shape is conical near the event horizon, we have

$$\begin{aligned} L_{\text{BZ}} &= 2\pi \int_0^{\theta_H} d\theta \mathcal{E}_H^r \Sigma_H \sin \theta \\ &= 2\pi \epsilon_0 \Psi_{\text{eq}}^2 \int_0^{\theta_H} d\theta \frac{2mr_H}{\Sigma_H} \Omega_F (\omega_H - \Omega_F) \sin^3 \theta, \end{aligned} \quad (31)$$

where  $\theta_H$  is the half opening angle of the jet at the event horizon. The magnetic flux function at the event horizon is assumed to  $\Psi(r_H, \theta) = \Psi_{\text{eq}}(1 - \cos \theta)$  with a constant  $\Psi_{\text{eq}}$ . The jet's opening angle is narrow enough,  $\theta_H \ll 1$ , such that the BZ power is estimated as follows:

$$\begin{aligned} L_{\text{BZ}} &\approx 3.3 \times 10^{38} \Lambda \frac{\Omega_F}{\omega_H} \left(1 - \frac{\Omega_F}{\omega_H}\right) \left(\frac{a}{m}\right)^2 \\ &\quad \times \left(\frac{B_{\text{pH}}}{0.1\text{T}}\right)^2 \left(\frac{m}{10^9 m_\odot}\right)^2 \text{J s}^{-1}, \end{aligned} \quad (32)$$

where  $\Lambda$  is the geometrical factor given by

$$\Lambda = \left(\frac{2}{3} - \frac{3}{4} \cos \theta_H + \frac{1}{12} \cos(3\theta_H)\right) = \frac{\theta_H^4}{4} + O(\theta_H^6). \quad (33)$$

Although we estimate  $\theta_0 \sim 1/\hat{E} \approx 0.1$  rad at the distant region from the BH, in the vicinity of the event horizon, the magnetic field lines for inflows would be parabolic [62,64] such that  $\theta_H > \theta_0 \sim 1/\hat{E}$ . So, when  $\theta_H \approx 0.3$  rad at the event horizon, we have  $\Lambda \approx 0.002$  as a rough value. Hence, for  $\Lambda = 0.002$ ,  $B_{\text{pH}} = 0.1$  T,  $m = m_{\text{M87}} = 6.5 \times 10^9 m_\odot$ ,  $a = 0.9m$ , and  $\Omega_F = 0.07\omega_H = 0.0219/m$ , we have  $L_{\text{BZ}} \approx 1.5 \times 10^{36} \text{J s}^{-1}$ , which agree with the value estimated by the jet observation. In Fig. 6, the value of  $\Omega_F$  was

estimated for the conical boundary wall; however, for the parabolalike boundary shape, the estimated  $\Omega_F$  value is about a factor larger. The BZ power may be an order of magnitude larger.

## VII. CONCLUDING REMARKS

In this article, we discussed the parameter dependence on the MHD outflows, and we realized that the solutions of  $u_{\text{inj}}^r > 0$  at  $r_{\text{inj}} = r_{\text{sp}}$  or  $r_{\text{sp}} < r_{\text{inj}}$  with  $u_{\text{inj}}^r = 0$ . That is, the initial velocity of the flow solution is not always 0, and the plasma sources may be widely distributed between the inner and outer light surfaces. Thus, the plasma source will have some internal structure; therefore, we should discuss some physical process for the plasma source. It may be some kind of plasma instabilities, nonideal MHD process, or particle pair-creation process [28–37]. By connecting the outflow solution obtained from the observation data to the plasma source, we can consider the junction condition or restrictions there (i.e., [27,65]). Further, we would discuss the inner BH magnetosphere. These details are outside the scope of this study and are for future study.

In this study, we define the nondimensional magnetic field  $\mathcal{B}_p$  and  $\mathcal{B}_\phi$ , and introduce the ratio  $\beta(r; \Psi)$  as a physical model. Therefore, there is no discussion about the particle number flux number  $\eta(\Psi)$  because this parameter is used to make  $\mathcal{B}_p$  and  $\mathcal{B}_\phi$  dimensionless, which is related to the fact that the critical condition at the magnetosonic points is no longer necessary in this model. To estimate  $\eta$  value, it is necessary to measure not only velocity distribution  $u^\alpha(r, \theta)$  but also magnetic field strength distribution  $B_p(r, \theta)$  and density distribution  $n(r, \theta)$ . Therefore, it is paramount to understand the mechanism of shock wave formation and the radiation mechanism in the jet region.

Thus, by comparing observational data, it is possible to quantitatively discuss the particle number flux  $\eta(\Psi)$ .

In summary, we applied the transfast magnetosonic outflow solution in a BH magnetosphere to the M87 jet. Specifically, we discussed the flow velocity  $u^r(Z; \Psi)$  and the magnetization parameter  $\sigma(Z; \Psi)$ . We evaluate the values of field-aligned flow parameters;  $\hat{E} \approx 10$ ,  $\tilde{L}\Omega_F \approx 0.9$ ,  $\Omega_F \approx (0.02 - 0.05)/m$ , i.e.,  $\Omega_F \approx (20 - 50) \text{ year}^{-1}$ . Using these values, the width of the outer light surface (light cylinder) is roughly  $R_L \approx (20 - 50)m$ , and the width of the Alfvén surface is roughly  $R_A \approx 0.95R_L$ . As the spatial resolution will be improved by future VLBI observations and the spatial distributions of jet velocity  $u^r(R, Z)$ , and the magnetic field strength are known, the distribution and limits of  $E(\Psi)$ ,  $L(\Psi)$ ,  $\Omega_F(\Psi)$ , and  $\eta(\Psi)$  will be revealed. Further, the future observations of the BH shadow by sub-millimeter wave and observations via other wavelengths, such as X- and gamma-ray, will also impose restrictions on the physical quantities of outflow and inflow. Thus, the quantitative understanding of BH magnetosphere including the plasma sources; hence, the BH spacetime, will be deepened.

## ACKNOWLEDGMENTS

The authors thank Honoka Daikai for fruitful discussions. M. T. was supported in part by JSPS KAKENHI Grant No. 17K05439. M. K. was supported in part by JSPS KAKENHI Grants No. JP18H03721 and No. JP21H01137. H.-Y.P. acknowledges the support of the Ministry of Education (MoE) Yushan Young Scholar Program, the Ministry of Science and Technology (MOST) under the Grant No. 110-2112-M-003-007-MY2, and National Taiwan Normal University.

- 
- [1] F. Mertens, A. P. Lobanov, R. C. Walker, and P. E. Hardee, Kinematics of the jet in M87 on scales of 100–1000 Schwarzschild radii, *Astron. Astrophys.* **595**, A54 (2016).
  - [2] K. Chatterjee, M. Liska, A. Tchekhovskoy, and S. B. Markoff, Accelerating AGN jets to parsec scales using general relativistic MHD simulations, *Mon. Not. R. Astron. Soc.* **490**, 2200 (2019).
  - [3] K. Asada and M. Nakamura, The structure of the M87 jet: A transition from parabolic to conical streamlines, *Astrophys. J. Lett.* **745**, L28 (2012).
  - [4] M. Nakamura and K. Asada, The parabolic jet structure in M87 as a magnetohydrodynamic nozzle, *Astrophys. J.* **775**, 118 (2013).
  - [5] K. Hada, M. Kino, A. Doi, H. Nagai, M. Honma, Y. Hagiwara, M. Giroletti, G. Giovannini, and N. Kawaguchi, The innermost collimation structure of the M87 jet down to  $\sim 10$  Schwarzschild radii, *Astrophys. J.* **775**, 70 (2013).
  - [6] J. Park *et al.*, Kinematics of the M87 jet in the collimation zone: Gradual acceleration and velocity stratification, *Astrophys. J.* **887**, 147 (2019).
  - [7] R. D. Blandford and R. L. Znajek, Electromagnetic extraction of energy from Kerr black holes, *Mon. Not. R. Astron. Soc.* **179**, 433 (1977).
  - [8] R. L. Znajek, Black hole electrodynamics and the Carter tetrad, *Mon. Not. R. Astron. Soc.* **179**, 457 (1977).
  - [9] M. Livio, G. I. Ogilvie, and J. E. Pringle, Extracting energy from black holes: The relative importance of the Blandford–Znajek mechanism, *Astrophys. J.* **512**, 100 (1999).
  - [10] V. S. Beskin and I. V. Kuznetsova, On the Blandford–Znajek mechanism of the energy loss of a rotating black hole, *Nuovo Cimento B* **115**, 795 (2000).
  - [11] M. Takahashi, S. Nitta, Y. Tatematsu, and A. Tomimatsu, Magnetohydrodynamic flows in Kerr geometry: Energy extraction from black holes, *Astrophys. J.* **363**, 206 (1990).

- [12] N. Globus and A. Levinson, Loaded magnetohydrodynamic flows in Kerr spacetime, *Phys. Rev. D* **88**, 084046 (2013).
- [13] M. Takahashi and S. Shibata, Trans-fast MHD winds in a pulsar magnetosphere, *Publ. Astron. Soc. Jpn.* **50**, 271 (1998).
- [14] M. Takahashi, Transmagnetosonic accretion in a black hole magnetosphere, *Astrophys. J.* **570**, 264 (2002).
- [15] T. Ogiwara, T. Ogawa, and K. Toma, Matter density distribution of general relativistic highly magnetized jets driven by black holes, *Astrophys. J.* **911**, 34 (2021).
- [16] M. Takahashi and A. Tomimatsu, Constraints on the evolution of black hole spin due to magnetohydrodynamic accretion, *Phys. Rev. D* **78**, 023012 (2008).
- [17] Z.-Y. Li, T. Chueh, and M. C. Begelman, Electromagnetically driven relativistic jets: A class of self-similar solutions, *Astrophys. J.* **394**, 459 (1992).
- [18] M. C. Begelman and Z.-Y. Li, Asymptotic domination of cold relativistic MHD winds by kinetic energy flux, *Astrophys. J.* **426**, 269 (1994).
- [19] S. Appl and M. Camenzind, Self-collimated jets beyond the light cylinder, *Astron. Astrophys.* **270**, 71 (1993).
- [20] Y. Lyubarsky, Asymptotic structure of Poynting-Dominated jets, *Astrophys. J.* **698**, 1570 (2009).
- [21] L. Huang, Z. Pan, and C. Yu, Toward a full MHD jet model of spinning black holes. II. Kinematics and application to the M87 jet, *Astrophys. J.* **894**, 45 (2020).
- [22] M. Camenzind, Hydromagnetic flows from rapidly rotating compact objects II. The relativistic axisymmetric jet equilibrium, *Astron. Astrophys.* **184**, 341 (1987).
- [23] S. Nitta, M. Takahashi, and A. Tomimatsu, Effects of magnetohydrodynamic accretion flows on global structure of a Kerr Black-Hole magnetosphere, *Phys. Rev. D* **44**, 2295 (1991).
- [24] V. S. Beskin, Axisymmetric stationary flows in compact astrophysical objects, *Phys. Usp.* **40**, 659 (1997).
- [25] M. Kino and M. Takahashi *et al.*, Signature of slowly rotating magnetosphere and magnetically arrested disk of the M87 jet (to be published).
- [26] A. Tomimatsu and M. Takahashi, Relativistic Acceleration of magnetically driven jets, *Astrophys. J.* **592**, 321 (2003).
- [27] H.-Y. Pu and M. Takahashi, Properties of trans-fast magnetosonic jets in black hole magnetospheres, *Astrophys. J.* **892**, 37 (2020).
- [28] M. Mościbrodzka, C. F. Gammie, J. C. Dolence, and H. Shiokawa, Pair production in low-luminosity galactic nuclei, *Astrophys. J.* **735**, 9 (2011).
- [29] G. N. Wong, B. R. Ryan, and C. F. Gammie, Pair drizzle around sub-Eddington supermassive black holes, *Astrophys. J.* **907**, 73 (2021).
- [30] N. Globus and A. Levinson, Jet formation in GRBs: A semi-analytic model of MHD flow in Kerr geometry with relativistic plasma injection, *Astrophys. J.* **796**, 26 (2014).
- [31] N. Globus and A. Levinson, Plasma injection and outflow formation in Kerr black holes, High energy phenomena in relativistic outflows (HEPRO IV), *Int. J. Mod. Phys.* **28**, 1460164 (2014).
- [32] V. S. Beskin, Y. N. Istomin, and V. I. Par'ev, Filling the magnetosphere of a supermassive black-hole with plasma, *Astron. Zh.* **69**, 1258 (1992) [*Sov. Astron.* **36**, 642 (1992)].
- [33] K. Hirotani and I. Okamoto, Pair plasma production in a force-free magnetosphere around a supermassive black hole, *Astrophys. J.* **497**, 563 (1998).
- [34] K. Hirotani and H.-Y. Pu, Energetic Gamma radiation from rapidly rotating black holes, *Astrophys. J.* **818**, 50 (2016).
- [35] A. Levinson and F. Rieger, Variable TeV Emission as a manifestation of jet formation in M87?, *Astrophys. J.* **730**, 123 (2011).
- [36] A. E. Broderick and A. Tchekhovskoy, Horizon-scale lepton acceleration in jets: Explaining the compact radio emission in M87, *Astrophys. J.* **809**, 97 (2015).
- [37] S. Kisaka, A. Levinson, and K. Toma, Comprehensive analysis of magnetospheric gaps around Kerr black holes using 1D GRPIC simulations, *Astrophys. J.* **902**, 80 (2020).
- [38] K. Parfrey, A. Philippov, and B. Cerutti, First-Principles Plasma Simulations of Black-Hole Jet Launching, *Phys. Rev. Lett.* **122**, 035101 (2019).
- [39] B. Crinquad, B. Cerutti, A. Philippov, K. Parfrey, and G. Dubus, Multi-Dimensional Simulations of Ergospheric Pair Discharges Around Black Holes, *Phys. Rev. Lett.* **124**, 145101 (2020).
- [40] J. D. Bekenstein and E. Oron, New conservation laws in general-relativistic magnetohydrodynamics, *Phys. Rev. D* **18**, 1809 (1978).
- [41] M. Camenzind, Centrifugally driven MHD-winds in active galactic nuclei, *Astron. Astrophys.* **156**, 137 (1986).
- [42] M. Camenzind, Hydromagnetic flows from rapidly rotating compact objects I. Cold relativistic flows from rapid rotators, *Astron. Astrophys.* **162**, 32 (1986).
- [43] M. Takahashi, D. Rilett, K. Fukumura, and S. Tsuruta, Magnetohydrodynamic shock conditions for accreting plasma onto Kerr black holes. I., *Astrophys. J.* **572**, 950 (2002).
- [44] M. Takahashi, J. Goto, K. Fukumura, D. Rilett, and S. Tsuruta, Standing shocks in transmagnetosonic accretion flows onto a black hole, *Astrophys. J.* **645**, 1408 (2006).
- [45] M. Takahashi and R. Takahashi, Black hole aurora powered by a rotating black hole, *Astrophys. J. Lett.* **714**, L176 (2010).
- [46] A. Tomimatsu, T. Matsuoka, and M. Takahashi, Screw instability in black hole magnetospheres and a stabilizing effect of field-line rotation, *Phys. Rev. D* **64**, 123003 (2001).
- [47] K. Gebhardt, J. Adams, D. Richstone, T. R. Lauer, S. M. Faber, K. Gültekin, J. Murphy, and S. Tremaine, The black hole mass in M87 from GEMINI/NIFS adaptive optics observations, *Astrophys. J.* **729**, 119 (2011).
- [48] K. Akiyama *et al.* (Event Horizon Telescope Collaboration), First M87 Event Horizon Telescope results. I. The shadow of the supermassive black hole, *Astrophys. J. Lett.* **875**, L1 (2019).
- [49] R. C. Walker, P. E. Hardee, F. B. Davies, C. Ly, and W. Junor, The structure and dynamics of the subparsec jet in M87 based on 50 VLBA observations over 17 years at 43 GHz, *Astrophys. J.* **855**, 128 (2018).
- [50] R. D. Blandford and D. G. Payne, Hydromagnetic flows from accretion discs and the production of radio jets, *Mon. Not. R. Astron. Soc.* **199**, 883 (1982).
- [51] Y.-R. Li, Y.-F. Yuan, J.-M. Wang, J.-C. Wang, and S. Zhang, Spins of supermassive black holes in M87. II. Fully general relativistic calculations, *Astrophys. J.* **699**, 513 (2009).

- [52] Y. Y. Kovalev, M. L. Lister, D. C. Homan, and K. I. Kellermann, The inner jet of the radio galaxy M87, *Astrophys. J. Lett.* **668**, L27 (2007).
- [53] K. Asada, M. Nakamura, A. Doi, H. Nagai, and M. Inoue, Discovery of sub- to superluminal motions in the M87 jet: An implication of acceleration from sub-relativistic to relativistic speeds, *Astrophys. J. Lett.* **781**, L2 (2014).
- [54] K. Hada *et al.*, High-sensitivity 86 GHz (3.5 mm) VLBI observations of M87: Deep imaging of the jet base at a resolution of 10 Schwarzschild-Radii, *Astrophys. J.* **817**, 131 (2016).
- [55] K. Hada, J. H. Park, M. Kino *et al.*, Pilot KaVA monitoring on the M 87 jet: Confirming the inner jet structure and superluminal motions at sub-pc scales, *Publ. Astron. Soc. Jpn.* **69**, 71 (2017).
- [56] J. C. McKinney, General relativistic magnetohydrodynamic simulations of the jet formation and large-scale propagation from black hole accretion systems, *Mon. Not. R. Astron. Soc.* **368**, 1561 (2006).
- [57] M. Nakamura, K. Asada, K. Hada *et al.*, Parabolic jets from the spinning black hole in M87, *Astrophys. J.* **868**, 146 (2018).
- [58] J. F. Mahlmann, P. Cerdá-Durán, and M. A. Aloy, Numerically solving the relativistic Grad-Shafranov equation in Kerr spacetimes: Numerical techniques, *Mon. Not. R. Astron. Soc.* **477**, 3927 (2018).
- [59] M. Kino, F. Takahara, K. Hada, and A. Doi, Relativistic electrons and magnetic fields of the M87 jet on the  $\sim 10$  Schwarzschild radii scale, *Astrophys. J.* **786**, 5 (2014).
- [60] M. Kino, F. Takahara, K. Hada, K. Akiyama, H. Nagai, and B. W. Sohn, Magnetization degree at the jet base of M87 derived from the event horizon telescope data: Testing the magnetically driven jet paradigm, *Astrophys. J.* **803**, 30 (2015).
- [61] V. A. Acciari *et al.* (MAGIC Collaboration), Monitoring of the radio galaxy M 87 during a low-emission state from 2012 to 2015 with MAGIC, *Mon. Not. R. Astron. Soc.* **492**, 5354 (2020).
- [62] K. Thoelecke, S. Tsuruta, and M. Takahashi, Effects of inner Alfvén surface location on black hole energy extraction in the limit of a force-free magnetosphere, *Phys. Rev. D* **95**, 063008 (2017).
- [63] S. S. Komissarov, General relativistic magnetohydrodynamic simulations of monopole magnetospheres of black holes, *Mon. Not. R. Astron. Soc.* **350**, 1431 (2004).
- [64] K. Thoelecke, M. Takahashi, and S. Tsuruta, The structure of magnetically dominated energy-extracting black hole magnetospheres: Dependencies on field line angular velocity, *Prog. Theor. Exp. Phys.* **2019**, 093E01 (2019).
- [65] H.-Y. Pu, M. Nakamura, K. Hirotani, Y. Mizuno, K. Wu, and K. Asada, Steady general relativistic magnetohydrodynamic inflow/outflow solution along large-scale magnetic fields that thread a rotating black hole, *Astrophys. J.* **801**, 56 (2015).